

A New Procedure for Evaluating Ground Motion Models, with Application to Hydraulic-Fracture-Induced Seismicity in the UK

(Revised submission to BSSA)

Gemma Cremen, Maximilian J. Werner, and Brian Baptie

December 2019

1 **Abstract**

2 An essential component of seismic hazard analysis is the prediction of ground shaking (and its uncertainty),
3 using ground motion prediction equations (GMPEs). This paper proposes a new method to evaluate (i.e.
4 rank) the suitability of GMPEs for modelling ground motions in a given region. The method leverages a
5 statistical tool from sensitivity analysis to quantitatively compare predictions of a GMPE with underlying
6 observations. We demonstrate the performance of the proposed method relative to several other popular
7 GMPE ranking procedures and highlight its advantages, which include its intuitive scoring system and its
8 ability to account for the hierarchical structure of GMPEs. We use the proposed method to evaluate the
9 applicability of several GMPEs for modelling ground motions induced by the commencement of UK shale gas
10 exploration, with 195 recordings at distances (R) less than 10 km for 29 events with local magnitude (M_L)
11 greater than 0 that relate to 2018/2019 hydraulic fracture operations at the Preston New Road shale gas
12 site in Lancashire and 192 $R < 10$ km recordings for 48 $M_L > 0$ events induced - within the same geologic
13 formation - by coal mining near New Ollerton, North Nottinghamshire. We examine: (1) the Akkar et al.
14 (2014a) equations for European seismicity, (2) the Douglas et al. (2013) equation for geothermal induced
15 seismicity, and (3) the Atkinson (2015) equation for eastern North America induced seismicity. We find
16 the Douglas et al. (2013) equation to be the most suitable for almost all of the considered ground motion

17 intensity measures. We modify this equation by re-computing its coefficients in line with the observed data,
18 to further improve its accuracy for future analyses of the seismic hazard of interest. This study both advances
19 the state of the art in ground motion model evaluation and enhances understanding of the seismic hazard
20 related to UK shale gas exploration.

21 **1 Introduction**

22 Ground motion prediction equations (GMPEs) are an essential component of seismic hazard analysis, used
23 to predict ground shaking at a given distance from a particular magnitude event. It is therefore important
24 that the GMPEs selected for inclusion in a given seismic hazard assessment are suitable for modelling the
25 ground motions in the region of interest. A variety of methods have been proposed in the literature for
26 evaluating (or ranking) GMPE suitability (e.g. Stewart et al., 2015). These include: (1) the analysis of
27 residuals (i.e. differences between observations and corresponding predictions of the GMPE), which involves
28 examining variations of the residuals with magnitude, distance, and site conditions (Scasserra et al., 2009),
29 (2) the use of a likelihood-based score (Scherbaum et al., 2004; Stafford et al., 2008), which involves assessing
30 the goodness-of-fit of the observations and the GMPE based on a likelihood parameter, and (3) the use of
31 information theory (Scherbaum et al., 2009; Mak et al., 2017), which involves calculating log-likelihoods of
32 observations for the GMPE. Interested readers are referred to Table 1 of Mak et al. (2017) for an excellent
33 summary of the various methods that have been used in an extensive number of previous GMPE evaluation
34 studies.

35 This paper proposes a new procedure for evaluating GMPEs. The method introduces a statistical tool
36 from sensitivity analysis to quantify (score) the comparison between the cumulative distribution function
37 (CDF) of residuals from a GMPE and the CDF expected if the equation correctly models the underlying
38 observations. The proposed procedure offers a number of advantages over current evaluation methods (dis-
39 cussed in detail in a later section of the paper). For example, it correctly accounts for the hierarchical
40 structure of GMPEs, i.e. the fact that they include correlation among ground motions from the same earth-
41 quake. It uses an intuitive scoring system, in which the optimum value is consistent; it does not depend
42 on either the GMPE under evaluation or the observed data of interest. It also involves the calculation of

43 residuals, which can act as a powerful visual tool to provide additional insight on how GMPEs compare with
44 observations.

45 We use the proposed GMPE evaluation procedure to help improve understanding of the seismic hazard
46 associated with shale gas exploration in the UK, where such industrial activity is relatively new; the first
47 well to specifically test for UK shale gas was drilled in 2010 (Selley, 2012), and the first recorded instance of
48 seismicity induced by hydraulic fracturing in the UK occurred in 2011 (Clarke et al., 2014). We specifically
49 focus on the Preston New Road (PNR) shale gas site near Blackpool in Lancashire (Clarke et al., 2019),
50 where the British Geological Survey (BGS) surface array detected 57 seismic events in 2018 and 121 seismic
51 events in 2019 (up to 27th August), related to hydraulic fracture operations. While the magnitudes of the
52 PNR events are significantly lower than those considered in conventional seismic hazard analyses, it is still
53 useful to assess whether the associated shaking has the potential to be felt.

54 We test a number of pre-existing GMPEs for suitability to modelling the ground motions induced by UK
55 shale gas exploration: (1) the Akkar et al. (2014a) equations, developed for European seismicity, (2) the
56 Douglas et al. (2013) equation, developed for induced seismicity in geothermal areas, and (3) the Atkinson
57 (2015) equation, developed for induced seismicity in eastern North America. Evaluation of the GMPEs is
58 specifically carried out for peak ground velocity (*PGV*), peak ground acceleration (*PGA*), and 5% damped
59 spectral accelerations at periods of 0.05s, 0.1s, and 0.2s ($SA_{0.05}$, $SA_{0.1}$, and $SA_{0.2}$ respectively). We then
60 adjust the coefficients of the most suitable GMPE, to create a model specific to the seismicity of interest so
61 that it can be used for future related hazard analyses (see **Developing a Modified GMPE** for details).

62 This paper is structured as follows. In **Proposed GMPE Evaluation Procedure**, we introduce the
63 proposed GMPE evaluation procedure, demonstrate its performance relative to other evaluation methods,
64 and describe its advantages as well as its limitations. In **Evaluating GMPEs for Modelling UK Shale
65 Gas Seismicity**, we use the proposed procedure to evaluate the suitability of the aforementioned GMPEs
66 for modelling ground shaking related to UK shale gas exploration. In **Developing a Modified GMPE**,
67 we modify the most applicable GMPE to better suit the UK data, and compare the adjusted model to the
68 previously examined GMPEs.

2 Proposed GMPE Evaluation Procedure

Ground motion prediction equations typically take the following mathematical form:

$$\log(im_{obs,i,j}) = \log(im_{GMPE,i,j}) + z_{E,i}\sigma_E + z_{A,i,j}\sigma_A \quad (1)$$

where - for the j th recording of the i th event - $\log(im_{obs,i,j})$ is the logarithm of the observed ground motion measure, $\log(im_{GMPE,i,j})$ is the logarithm of the median estimate of the ground motion measure given certain predictor variables (e.g. magnitude and distance) and model parameters, $z_{E,i}$ is the normalised inter-event residual (common to all recordings of the i th event), $z_{A,i,j}$ is the normalised intra-event residual, and σ_E and σ_A are the inter-event and intra-event standard deviations, respectively. $z_{E,i}$ can be estimated using (Abrahamson and Youngs, 1992):

$$z_{E,i} = \frac{\sigma_E \times \sum_{j=1}^{n_i} [\log(im_{obs,i,j}) - \log(im_{GMPE,i,j})]}{n_i\sigma_E^2 + \sigma_A^2} \quad (2)$$

where n_i is the number of recordings for the i th event. $z_{A,i,j}$ can then be calculated from:

$$z_{A,i,j} = \frac{\log(im_{obs,i,j}) - \log(im_{GMPE,i,j}) - z_{E,i}\sigma_E}{\sigma_A} \quad (3)$$

The format of equation 1 implies that both $z_{E,i}$ and $z_{A,i,j}$ should follow a standard normal distribution (i.e. mean=0, standard deviation =1) if the GMPE correctly models the observed data; this forms the basis of our proposed evaluation procedure. We use the Euclidean metric distance (EMD) between the cumulative distribution function (CDF) of the standard normal distribution and that of the maximum likelihood normal distribution for each type of normalised residual, to score models. This metric has previously been used to quantify uncertainty importance for sensitivity analyses (Chun et al., 2000). It may be calculated as follows:

$$EMD_x = \sqrt{(\mu_x - \mu_o)^2 + (\sigma_x - \sigma_o)^2} = \sqrt{\mu_x^2 + (\sigma_x - 1)^2} \quad (4)$$

where x refers to the normalised inter- or intra- event residuals, μ_x and σ_x are the maximum likelihood

86 estimates of the mean and standard deviation, respectively, for the normalised residuals, and μ_o and σ_o
87 are respectively the mean and standard deviation of the standard normal distribution. Note that equation
88 4 assumes the distribution of normalised residuals to be symmetric; the generic equation for the distance
89 between any two CDFs is presented in equation 2 of Chun et al. (2000). The assumption of symmetric data
90 is reasonable, since it is also the fundamental underlying assumption of a GMPE (from equation 1) and it is
91 always valid (for sufficient sample sizes), based on the Central Limit Theorem (Kwak and Kim, 2017).

92 A graphical representation of EMD_x is provided in Figure 1. The final score for the proposed evaluation
93 procedure (EMD_{total}) is a combination of the inter- and intra- event Euclidean metric distances, as follows:

94

$$EMD_{total} = \sqrt{EMD_{inter}^2 + EMD_{intra}^2} \quad (5)$$

95 The smaller the score, the closer the residuals are to the ideal distribution and the better the model. The
96 format of equation 5 assumes that the errors from both types of residual are additive, independent, and
97 equally important, which is directly consistent with the treatment of inter- and intra-event variabilities
98 within GMPEs (e.g. Ornthammarath et al., 2011).

99 The proposed EMD scoring method is not to be confused with the Euclidean distance-based ranking
100 (EDR) procedure proposed by Kale and Akkar (2013) , which is fundamentally different in its methodology.
101 The EDR approach measures the Euclidean distance directly between an observed ground motion amplitude
102 and the corresponding probability distribution of predictions from a GMPE, whereas the EMD method first
103 calculates normalised residuals based on the median prediction of a GMPE; then measures the Euclidean
104 distance between the probability distribution of residuals and the standard distribution expected for a perfect
105 prediction by the model (which is independent of the GMPE in question). The proposed EMD score has
106 a number of advantages over the EDR score: (1) the EMD score is proper, (2) residuals are a natural
107 by-product of calculating the EMD score, which can provide additional useful insight on the performance
108 of a GMPE, and (3) the EMD score accounts for model hierarchy in GMPEs by considering inter- and
109 intra-event variability separately. Further discussion on these advantages is left to

110 **Advantages and Limitations of the Proposed Procedure**, where the benefits of the EMD approach
111 over other popular GMPE ranking methods are also explained.

112 2.1 Extension to Non-Constant Inter- and Intra-Event Standard Deviations

113 It is important to note that equations 2 and 3 are only valid if the inter- and intra-event standard deviations
 114 of a GMPE are constant (homoskedastic) across all values of the predictor variables (Stafford, 2015), which
 115 is not always the case (e.g. Ambraseys et al., 2005; Akkar and Bommer, 2007; Chiou and Youngs, 2014).
 116 The normalised inter-event residual vector for scenario-dependent inter- and intra-event standard deviations
 117 may be formulated as (Laird, 2004):

$$\mathbf{z}_{\mathbf{E},i} = \mathbf{D}^{0.5} \mathbf{Z}'_i \boldsymbol{\Sigma}_i^{-1} [\log(\mathbf{im}_{\text{obs},i}) - \log(\mathbf{im}_{\text{GMPE},i})] \quad (6)$$

118 where, for the i th earthquake, \mathbf{D} is the inter-event covariance matrix and \mathbf{Z}_i describes the linear relation of
 119 random effects (note that \mathbf{Z}'_i denotes the transpose of \mathbf{Z}_i). $\log(\mathbf{im}_{\text{obs},i})$ and $\log(\mathbf{im}_{\text{GMPE},i})$ are vectors (in
 120 logarithmic scale) of the observed and median estimates of the ground motion measures, respectively. $\boldsymbol{\Sigma}_i$
 121 can be calculated as follows:

$$\boldsymbol{\Sigma}_i = \mathbf{R}_i + \mathbf{Z}_i \mathbf{D} \mathbf{Z}'_i \quad (7)$$

122 where \mathbf{R}_i is the intra-event covariance matrix for the i th earthquake, and both \mathbf{Z}_i and \mathbf{D} are as described
 123 for equation 6. The normalised intra-event residual vector for scenario-dependent inter- and intra-event
 124 standard deviations is then calculated as:

$$\mathbf{z}_{\mathbf{A},i} = \mathbf{R}_i^{-0.5} [\log(\mathbf{im}_{\text{obs},i}) - \log(\mathbf{im}_{\text{GMPE},i}) - \mathbf{D}^{0.5} \mathbf{z}_{\mathbf{E},i}] \quad (8)$$

125 where all other variables are as defined previously. $\mathbf{z}_{\mathbf{E},i}$ and $\mathbf{z}_{\mathbf{A},i}$ should follow standard multivariate normal
 126 distributions if the GMPE is a correct model for the observations. Extension of the EMD_{total} metric to
 127 quantify the distance between the maximum likelihood multivariate normal distribution of the residuals
 128 and the standard multivariate normal distribution could be achieved using tools from optimal transport
 129 theory (e.g. Villani, 2008). However, since all the GMPEs to be evaluated in this study have homoskedastic
 130 standard deviations, further discussion on the ranking of GMPEs with scenario-dependent inter- and intra-
 131 event variabilities is left for future work.

2.2 Advantages and Limitations of the Proposed Procedure

To demonstrate the relative performance of the proposed procedure, we use the synthetic datasets of Mak et al. (2017), i.e. we assume there are four earthquakes with event terms η_i , $i \in \{1, 2, 3, 4\}$ that uniformly sample the distribution $\mathcal{N}(0, \sigma_b)$ and the N_i records for each earthquake uniformly sample the distribution $\mathcal{N}(\eta_i, \sigma_w)$. Thus, the j th residual for the i th event is calculated as:

$$r_{i,j} = Q_w(y_j) + \eta_i \quad (9)$$

where $y_j = \frac{2j-1}{2N_i}$, $j \in \{1, 2, \dots, N_i\}$, $\eta_i = Q_b(x_i)$ with $x_i = \frac{2i-1}{8}$, and $Q_c(\cdot)$ is the quantile function for $\mathcal{N}(0, \sigma_c)$. We also make use of Examples 1-3 of Mak et al. (2017), which compare the performance of different scores in various scenarios. Example 1 examines the variability of scores for perfect models across similar cases: (1) $N_i = \{20, 5, 5, 20\}$ and (2) $N_i = \{5, 20, 20, 5\}$ with $\sigma_b = 0.35$ and $\sigma_w = 0.5$. Example 2 examines the performance of scores using $N_i = \{10, 10, 10, 50\}$, $\sigma_b = 0.35$, $\sigma_w = 0.5$, and a biased model. Example 3 examines the ability of scores to distinguish between the correct and incorrect model partitioning of total uncertainty into inter-event and intra-event uncertainties for Case 1 of Example 1.

While these examples are useful for highlighting the pros and cons of the proposed procedure, it is important to emphasise their hypothetical (unrealistic) nature. Imbalances in the number of recordings per earthquake are over-exaggerated, as mentioned in Mak et al. (2017). In addition, sample sizes are exceptionally small (for instance, we note that Bommer et al. (2010) recommends at least 10 earthquakes per unit of magnitude and at least 100 records per 100 km to adequately constrain a GMPE) and an accurate evaluation of GMPEs may not be the only challenge to overcome when analysing such a limited amount of data. Actual datasets of this scale have led to difficulties in successfully calculating inter- and intra-event residuals (Bourne et al., 2015), for instance.

2.2.1 Advantages

The proposed evaluation procedure provides numerous benefits over similar methods previously proposed in the literature. The proposed score has three main advantages over both the \overline{LLH} score proposed by

155 Scherbaum et al. (2009) and the the *EDR* score proposed by Kale and Akkar (2013). (1) The proposed
 156 score is proper (Lindley, 1991), since the best (lowest) score is achieved when the GMPE perfectly fits the
 157 observed data, i.e. when the CDFs of the residuals exactly match that of the standard normal distribution.
 158 On the other hand, the \overline{LLH} score can favour a biased model if the number of recordings is unbalanced
 159 between earthquakes (Mak et al., 2017) and the *EDR* score favours a smaller predicted uncertainty value,
 160 regardless of what the true uncertainty is, when the predicted mean is close to correct (Mak et al., 2014). We
 161 demonstrate this benefit of the proposed score using the data of Example 2 in Mak et al. (2017). Unlike the
 162 \overline{LLH} score, the proposed procedure correctly assigns a better score to the unbiased model (EMD_{total} for
 163 the correct model is 0.25 and EMD_{total} for the biased model is 0.48). If we halve both the inter-event (σ_b)
 164 and intra-event (σ_w) standard deviations of the correct model while keeping the observations unchanged,
 165 the proposed score disimproves from 0.25 to 1.04, whereas the *EDR* score incorrectly improves from 0.72
 166 to 0.62. (2) Residuals are also calculated as part of obtaining the *EDR* score, which can provide additional
 167 insight on whether a GMPE is high or low relative to the observed data of interest (e.g. Bradley, 2013).
 168 (3) Through the separate consideration of intra- and inter-event residuals, the proposed procedure correctly
 169 accounts for the hierarchical nature of ground motion prediction equations, whereas the \overline{LLH} score and the
 170 *EDR* score do not distinguish between these two types of variability.

171 The *EMD* approach has a number of advantages over the $\ell\ell(\mathbf{p}, \mathbf{V}, \mathbf{q})$ score proposed by Mak et al. (2017),
 172 which (to the best of our knowledge) is the only other score that incorporates model hierarchy. Firstly, the
 173 proposed score is more intuitive than the $\ell\ell(\mathbf{p}, \mathbf{V}, \mathbf{q})$ score, since its best possible value is always 0 whereas
 174 the $\ell\ell(\mathbf{p}, \mathbf{V}, \mathbf{q})$ score has a variable optimum value that depends on the length of the given dataset (via the
 175 ‘ $N \log(2\pi)$ ’ term) and the variance of the model to be evaluated (via the ‘ $\log |\mathbf{V}| + (\mathbf{q} - \mathbf{p})' \mathbf{V}^{-1} (\mathbf{q} - \mathbf{p})$ ’
 176 terms). The variability of the optimum $\ell\ell(\mathbf{p}, \mathbf{V}, \mathbf{q})$ score is highlighted in Example 2 and Example 3 of Mak
 177 et al. (2017); the score for the correct model in Example 2 (where there are 4 earthquakes and 80 records) is
 178 61.2, whereas the score for the correct model in Example 3 (where there are 4 earthquakes and 50 records)
 179 is 38.8. (The EMD_{total} score for both models is 0.25). Secondly, the proposed procedure is significantly
 180 less computationally expensive than that proposed by Mak et al. (2017) (at least when evaluating GMPEs
 181 with homoskedastic standard deviations); it only requires space for $\sum_{i=1}^{n_e} n_{r_i} + n_e$ residuals (where n_e is

182 the number of earthquakes and n_{r_i} is the number of records for the i th earthquake) plus the maximum
183 likelihood estimates of the residual distributions, whereas the procedure of Mak et al. (2017) necessitates the
184 storage of $\sum_{i=1}^{n_e} n_{r_i}^2$ non-zero elements for the \mathbf{V} matrix alone. To demonstrate the practical significance of
185 the difference in computational requirements between the two methods, we use a hypothetical dataset with
186 100 earthquakes and 100 records per earthquake - which roughly corresponds in record number to half the
187 size of the NGA West-2 ground motion database (Ancheta et al., 2014) - and assume that we are evaluating
188 a GMPE with homoskedastic standard deviation. For double precision in the MATLAB environment, the
189 procedure of Mak et al. (2017) will require 800 MB of storage for the \mathbf{V} matrix, whereas the necessary
190 data for the proposed procedure can be stored in a vector of less than 0.1 MB in size. The computational
191 advantage of the proposed procedure will become even more apparent as future evaluations of models involve
192 increasing amounts of recorded data.

193 The proposed score also has an advantage over goodness-of-fit measures proposed for evaluating GMPEs
194 - such as the Kolmogorov-Smirnov test and the mean test p-value (Scherbaum et al., 2004) - since it does
195 not include the use of classical statistical hypothesis testing, which can be limited in ability to measure the
196 importance of a result (Wasserstein and Lazar, 2016).

197 **2.2.2 Sample Size Constraints**

198 To assess the reliability of the proposed procedure for modest sample sizes, we compute scores for the small
199 datasets examined in Examples 1-3 of Mak et al. (2017), which contain 50-80 records across 4 earthquakes.
200 It can be observed from Table 1 that the proposed procedure correctly scores the models in Example 2 (as
201 discussed in **Advantages**) but it does not perform as expected for Examples 1 and 3; the scores are not
202 equivalent for both (correct) cases in Example 1, and the model with the smallest σ_b is incorrectly deemed to
203 be the best in Example 3. The incorrect scoring in Examples 1 and 3 is due to the inaccurate estimation of
204 inter-event residuals by equation 2, which only represents the best predictor of random effects given the set of
205 available observations (Jiang, 2007). For instance in Example 1, inter-event residuals for Case 1 are estimated
206 to be $\{-1.04, -0.23, 0.23, 1.04\}$ and for Case 2 are estimated to be $\{-0.82, -0.29, 0.29, 0.82\}$, whereas the
207 true inter-event residuals for both cases (simulated according to equation 9) are $\{-1.15, -0.32, 0.32, 1.15\}$.

208 The incorrect scoring by the proposed procedure can also be minorly attributed to the use of maximum
 209 likelihood estimation for obtaining the means and standard deviations of the normalised residuals, which is
 210 well known to have reduced accuracy for small sample sizes (e.g. Lee and Song, 2004). We note that many
 211 other popular GMPE evaluation scores - such as that of Mak et al. (2017) as well as the Scherbaum et al.
 212 (2009) \overline{LLH} score - involve maximum likelihood estimates and are therefore also somewhat impacted by
 213 small sample sizes (Beauval et al., 2012).

214 To understand the sample sizes necessary for the proposed evaluation procedure to perform correctly in
 215 Examples 1 and 3, we calculate the scores for datasets with an increasing number of events and recordings
 216 (Figure 2). Increasing ‘Earthquake Number’ involves adding earthquakes to the centre (Case 1 in Example
 217 1 and Example 3) or outside (Case 2 in Example 1) of a dataset, with the same number of records as the
 218 nearest events in the set. Increasing ‘Record Number Scaling’ involves multiplying the number of records per
 219 earthquake by a factor. For example, an ‘Earthquake Number’ of 10 and a ‘Record Number Scaling’ of 2 for
 220 Case 1 in Example 1 yields the dataset $N_i = \{40, 10, 10, 10, 10, 10, 10, 10, 10, 10, 40\}$, and for Case 2 in Example
 221 1 yields the dataset $N_i = \{10, 10, 10, 10, 40, 40, 10, 10, 10, 10\}$. Residuals are still calculated according to
 222 equation 9, with the denominator of x_i replaced by $2 \times \text{Earthquake Number}$.

223 Figure 2a plots the absolute difference between the EMD_{total} values for Case 1 and Case 2 in Example
 224 1, and Figure 2b plots the difference between the EMD_{total} values for the correct model and the model with
 225 deflated σ_b . It can be seen in Figure 2a that the absolute difference in EMD_{total} values for both cases in
 226 Example 1 will reduce to 0.01 if the number of records for each earthquake is scaled by 22 (1100 total records
 227 per case), or if the number of earthquakes is increased to 30 and the number of records per earthquake is
 228 scaled by 9 (1620 total records per case), for example. The proposed procedure will score the correct model
 229 better than the model with smallest σ_b in Example 3 if the number of earthquakes is increased to 10 and
 230 the number of records per earthquake is scaled by 4 (320 total records), or if the number of earthquakes is
 231 increased to 30 and the number of records for each earthquake is scaled by 3 (540 total records), for example
 232 (Figure 2b). It can be concluded that the number of earthquakes and recordings necessary for the proposed
 233 evaluation procedure to perform reliably for Examples 1 and 3 is notably larger than that examined by
 234 Mak et al. (2017), however we again emphasise that these examples are far from those expected in real-life

235 applications.

236 **3 Evaluating GMPEs for Modelling UK Shale Gas Seismicity**

237 We use the proposed GMPE evaluation procedure to help improve understanding of the seismic hazard
238 related to shale gas exploration in the UK, where such industrial activity is relatively new. We focus on
239 2018 and 2019 seismic events associated with the PNR shale gas site near Blackpool in Lancashire (Figure
240 4a), which are the only well-recorded series of shale gas-related events that have occurred in the UK. We
241 also use a high quality dataset of ground motion recordings from events that were induced by coal mining
242 near New Ollerton (NO) in North Nottinghamshire (Figure 4b; Verdon et al., 2017), as these earthquakes
243 had very similar magnitudes and depths to those of the PNR sequence (Figures 4c and 4d), they occurred
244 in the same geological formation (Butcher et al., 2017), and were found to have comparable ground motion
245 amplitudes to those of the 2018 PNR events for most of the intensity measures of interest (Cremen et al.,
246 2019).

247 **3.1 GMPEs Examined**

248 We evaluate the suitability of various GMPEs for modelling the ground motions of interest: (1) Akkar et
249 al. (2014a, hereafter ASB14), (2) Douglas et al. (2013, hereafter D13) and (3) Atkinson (2015, hereafter
250 A15). ASB14 was chosen because they were used for planning purposes in preliminary shale gas-related PNR
251 hazard calculations (Arup, 2014). D13 and A15 were chosen for their application to induced seismicity.

252 ASB14 are a series of GMPEs developed for European and Middle East crustal seismicity that were
253 derived using a subset of the Reference Database for Seismic Ground-Motion in Europe (RESORCE) (Akkar
254 et al., 2014b). They are applicable for moment magnitudes (M_w) greater than 4 and distances less than 200
255 km. The equations use either point-source (i.e. epicentral and hypocentral distance) or finite-fault (surface
256 projection of rupture distance) distance metrics. Events are sufficiently small such that rupture distance is
257 not important in this study, so we only use the point-source equations (henceforth referred to as ASB14_{hypo}
258 and ASB14_{epi}).

259 D13 are a series of GMPEs developed for geothermal induced seismicity that were derived using data

260 from induced and natural seismicity in Basel (Switzerland), Campi Flegrei (Italy), Geysers (United States),
261 Hengill (Iceland), Roswinkel and Vorendaal (the Netherlands), and Soultz-sous-Forets (France). They are
262 applicable for M_w greater than 1 and distances less than 50 km. All equations except one are site corrected
263 to a reference rock condition ($V_{s30} = 1100$ m/s). This condition is significantly different to that observed
264 at sites in this study ($V_{s30} = 280$ m/s, as explained in **Data Used**), so we only use the equation that
265 represents an unknown site condition in this case. (Note that we could make our data compatible with
266 the site corrected condition by obtaining site-specific estimates of amplification and attenuation, but this is
267 outside the scope of the current study.)

268 A15 is a GMPE developed for induced seismicity in eastern North America that was derived using a
269 subset of the Next Generation Attenuation-West 2 (NGA-West 2) database (Ancheta et al., 2014). It is
270 applicable for magnitudes between 3 and 6 and distances less than approximately 50 km. The equation is
271 site corrected to a reference soft rock condition ($V_{s30} = 760$ m/s). However, it can be conveniently adjusted
272 to another site condition by inputting the appropriate V_{s30} value to the empirical site correction model of
273 Seyhan and Stewart (2014), which was calibrated using the same database. We use this model to site correct
274 our data.

275 3.2 Data Used

276 We only examine data recorded at distances less than 10 km from events with local magnitude (M_L) > 0
277 in this study, since smaller magnitude events and farther locations (for the magnitude range considered in
278 this study) will have extremely low levels of shaking that will not be felt. 29 Preston New Road (PNR)
279 events fit the magnitude criterion, for which there are 76 recordings available within 10 km from nine Guralp
280 3-ESP broadband seismometers deployed by the BGS near the site. A further 119 recordings are available
281 for 2018 events from eight seismic instruments (two Kinometrics Shallow Borehole Episensor 2 broadband
282 accelerometers and six Geospace Technologies SNG 3C GS-ONE LF geophones) used for monitoring by the
283 shale gas exploration operator at the site, Cuadrilla Resources Ltd. We retrieve the event phase data and
284 the raw waveforms of the BGS instruments from the BGS seismic database, and the raw waveforms of the
285 operator’s instruments from the UK Oil and Gas Authority (see Data and Resources). We consider 48 New

286 Ollerton (NO) earthquakes greater than 0 M_L , for which there are 192 recordings available within 10 km
 287 from four Guralp 3-ESP broadband seismometers installed by the BGS. Waveforms and phase data for the
 288 earthquakes are accessed using the BGS seismic database. A histogram of the complete database is provided
 289 in Figure 3.

290 We convert waveforms from dimensions of digital counts to velocity or acceleration using the procedure
 291 of Haney et al. (2012) (for broadband seismometers), assuming a causal third-order high-pass Butterworth
 292 filter with frequency 3 Hz, a causal fifth-order low-pass Butterworth filter with frequency 20 Hz, and an
 293 oversampling rate of 5. Accelerations are obtained from the derived velocities by numerical differentiation,
 294 and velocities are obtained from the derived accelerations using numerical integration. Spectral accelerations
 295 are computed using the algorithm provided in Wang (1996). Ground motion intensities are calculated across a
 296 time window from p-wave arrival to 5 seconds after the occurrence of the maximum displacement amplitude.
 297 Signal-to-noise ratios for each seismogram are taken as a ratio of the Fourier amplitude spectrum (FAS)
 298 evaluated during this time window to the FAS evaluated for a noise window of equivalent duration (Perron
 299 et al., 2018). We ignore data with signal-to-noise ratios less than or equal to 3, which removes 3 $SA_{0.05}$
 300 values, 7 $SA_{0.1}$ values and 5 $SA_{0.2}$ values from the PNR dataset, and 1 $SA_{0.05}$ value from the NO dataset.
 301 The data considered for both earthquake sequences are summarised in Figure 4. It is important to note that
 302 the size of the dataset - 77 earthquakes with a median of 4 and a maximum of 12 data points per earthquake-
 303 is sufficient for the proposed evaluation procedure to perform correctly. We can confirm this by repeating
 304 Example 3 of Mak et al. (2017), using $N_i = \{x_i, x_{i+1}, \dots, x_{n-1}, x_n\}$, where the length (n) of $N_i = 77$ and
 305 x_i is equal to the number of records available for the i th earthquake. To adequately capture the interaction
 306 between sample size and event term, the earthquakes are placed within N_i in ascending order of their inter-
 307 event residual with respect to the $ASB14_{\text{hyppo}}$ GMPE. We find that the EMD_{total} scores accurately indicate
 308 the correct model; EMD_{total} for the correct model is 0.316, which is lower than the value for the model with
 309 inflated σ_b (0.332) and the value for the model with deflated σ_b (0.321).

310 The value of a ground motion intensity measure used for a particular event and distance combination
 311 depends on the requirements of the GMPE of interest. For $ASB14_{\text{hyppo}}$, $ASB14_{\text{epi}}$, and D13, it is taken as
 312 the geometric mean of the values computed for the two horizontal components. For A15, it is taken as the

313 median value for the two horizontal components computed over all nonredundant azimuths, as detailed in
 314 Boore (2010). M_L values are converted to M_w values using the empirical relationship derived by Butcher
 315 et al. (2019) for coal-mining induced seismicity in the UK:

$$M_w = 0.69M_L + 0.74 \quad (10)$$

316 All sites sit on alluvial soils so we use a V_{s30} value of 280 m/s, the median value found for these types of soil
 317 by Campbell et al. (2016), for site correction factors in ASB14_{hyppo}, ASB14_{epi}, and A15. We assume a linear
 318 site response for A15. We assume strike-slip style-of-faulting for PNR data and reverse faulting for NO data
 319 in ASB14_{hyppo} and ASB14_{epi}, as these are the respective dominant regimes for each type of seismicity (Clarke
 320 et al., 2019; Verdon et al., 2017).

321 **3.3 Evaluation Results**

322 Table 2 provides EMD_{total} scores for each GMPE. Also provided for comparison are $\ell\ell(\mathbf{p}, \mathbf{V}, \mathbf{q})$ scores,
 323 calculated according to the evaluation procedure proposed by Mak et al. (2017). Figures 5 and 6 provide the
 324 corresponding inter- and intra-event residuals, as well as those expected for a standard normal distribution
 325 (i.e. a perfectly fitting GMPE). It can be seen from Table 2 that, according to the proposed evaluation
 326 procedure, D13 is the most suitable GMPE for modelling all ground motion intensities examined except
 327 $SA_{0.2}$, for which A15 is the most suitable. It is interesting to note that these findings are consistent
 328 with those of a similar evaluation study carried out by Cremen et al. (2019) for the same GMPEs, which
 329 included only 2018 PNR data from the BGS seismometers and used the GMPE ranking scheme of Scherbaum
 330 et al. (2004). Since both ASB14 equations and A15 were calibrated at much higher magnitudes than those
 331 examined here (see **GMPEs Examined**), these results provide further support for previous studies, (e.g.
 332 Bommer et al., 2007; Douglas and Jousset, 2011; Atkinson and Morrison, 2009) which found that GMPEs
 333 derived from larger-magnitude events should not be extrapolated to predict ground motions from earthquakes
 334 with smaller magnitudes.

335 The ranking of GMPEs according to the proposed procedure matches that of the Mak et al. (2017)
 336 procedure except in the case of PGV , for which the proposed procedure favours D13 and the procedure of

337 Mak et al. (2017) favours A15. Figure 5 highlights why the proposed procedure favours D13 for *PGV*; while
 338 the intra-event residuals for A15 compare better overall with the standard normal distribution than those of
 339 D13 due to the closer fit of their standard deviation (mean of D13 intra-event residuals = -0.03 and mean of
 340 A15 intra-event residuals = 0.31, while standard deviation of D13 intra-event residuals = 0.41 and standard
 341 deviation of A15 intra-event residuals = 1.02), the inter-event residuals for D13 perform significantly better
 342 relative to the standard normal distribution than those of A15 due to their notably lower bias (mean of D13
 343 inter-event residuals = -0.06 and mean of A15 inter-event residuals = 1.10, while standard deviation of D13
 344 inter-event residuals = 0.30 and standard deviation of A15 inter-event residuals = 0.50). The Mak et al.
 345 (2017) procedure’s preference for A15 can be explained by A15’s significantly smaller variance relative to
 346 that of D13 for *PGV*; A15 intra-event variability for *PGV* (in natural log units) is 0.645, which is over 60%
 347 less than the equivalent value of 1.811 for D13. Even though the error term (i.e. $[\mathbf{q} - \mathbf{p}]'\mathbf{V}^{-1}[\mathbf{q} - \mathbf{p}]$) of the
 348 $\ell\ell(\mathbf{p}, \mathbf{V}, \mathbf{q})$ score is much lower for D13 (73) than A15 (551), the difference in values of the variance term (i.e.
 349 $\log |\mathbf{V}|$) is sufficient to yield an overall lower $\ell\ell(\mathbf{p}, \mathbf{V}, \mathbf{q})$ score for A15 ($\log |\mathbf{V}|$ is 505 for D13 and is -276 for
 350 A15).

351 4 Developing a Modified GMPE

352 We now analyse the suitability of the most promising GMPE, D13, in greater detail. This equation has the
 353 following functional form:

$$\ln Y = a + bM + c \ln \sqrt{r_{hyp}^2 + h^2} + dr_{hyp} + \mathcal{N}(0, \phi) + \mathcal{N}(0, \tau) \quad (11)$$

354 where Y is the observed ground motion intensity measure of interest for moment magnitude M and hypocen-
 355 tral distance (in km) r_{hyp} , $\mathcal{N}(\mu, \Sigma)$ is a normal distribution with mean μ and standard deviation Σ , ϕ is
 356 the intra-event standard deviation, τ is the inter-event standard deviation, and $\sigma = \sqrt{\phi^2 + \tau^2}$ is the total
 357 standard deviation.

358 We examine trends in the residuals with the different predictor variables and update model coefficients
 359 to better suit the data as required, similar to the referenced empirical method for fitting GMPEs (Atkinson,

2008) and in line with the procedure detailed in Scasserra et al. (2009). We first investigate the variation of
intra-event residuals ($\epsilon_{i,j}$) as a function of hypocentral distance (Figure 7). To highlight trends, we perform
a linear regression according to:

$$\epsilon_{i,j} = z_{A,i,j}\sigma_A = a_R + b_R R_{i,j} + (\epsilon_R)_{i,j} \quad (12)$$

where $z_{A,i,j}$ and σ_A are as defined in equation 3, $R_{i,j}$ is hypocentral distance, a_R and b_R are regression
parameters, and $(\epsilon_R)_{i,j}$ is the residual for the j th recording from the i th event. The p-values plotted in
Figure 7 test the null hypothesis that the slope parameter b_R is equal to zero; since they all have extremely
low values (i.e. ≤ 0.01), we can conclude that there is a statistically significant relationship between the
residuals and hypocentral distance for each ground motion intensity measure examined. b_R is negative in
each case, indicating that there is faster distance attenuation of the observed data relative to the D13 GMPE.
To address the distance attenuation discrepancy, we recalculate coefficients related to near-source saturation
(i.e. c and h) and the constant term of D13, using non-linear regression of the observed data. (We do not
attempt to reevaluate the anelastic attenuation term of D13, given the short distances of interest). Note that
the h coefficient is not found to be statistically significant in the initial regression analyses for any ground
motion intensity measure examined, so the values for the other two terms are instead computed with h set
to 0. We obtain the inter- and intra-event standard deviations of the distance-modified D13 by performing
mixed effects regression on the total log residuals $\log(Z_{i,j})$ (e.g. Scasserra et al., 2009), calculated as follows:

$$\log(Z_{i,j}) = \log(im_{obs,i,j}) - \log(im_{GMPE',i,j}) \quad (13)$$

where $\log(im_{GMPE',i,j})$ is the logarithm of the median estimate of the ground motion measure for the
model parameters of the distance-modified D13 and $\log(im_{obs,i,j})$ is as defined in equation 1. There is a
statistically insignificant relationship between the normalised intra-event residuals of the distance-modified
D13 and hypocentral distance (Figure 8), indicating that the updated GMPE is adequately capturing the
distance attenuation of the observed data.

We assess the magnitude-scaling of the distance-modified D13 by investigating the variation of the inter-

383 event residuals (η_i) as a function of moment magnitude (Figure 9). To illustrate trends, we conduct a linear
384 regression according to:

$$\eta_i = z_{E,i}\sigma_E = a_M + b_M M_i + (\epsilon_M)_i \quad (14)$$

385 where $z_{E,i}$ and σ_E are as defined in equation 2, M_i is moment magnitude, a_M and b_M are regression
386 parameters, and $(\epsilon_M)_i$ is the residual for the i th event. There is a statistically significant positive trend in
387 the residuals with moment magnitude for each ground motion intensity measure of interest besides *PGA*
388 (indicated by the small p-values for b_M plotted in Figure 9). This implies that the magnitude-scaling of the
389 observed data is larger than that predicted by the GMPE in these cases, which makes sense given that D13
390 was calibrated for slightly higher magnitudes (e.g. Chiou et al., 2010). To rectify this, we use linear regression
391 to recompute the magnitude-related coefficient and the constant term of the distance-modified D13 (except
392 in the case of *PGA*). Mixed-effects regression is then used to calculate the updated inter- and intra-event
393 standard deviations of the distance- and magnitude-modified D13. It is observed in Figure 10 that the
394 distance- and magnitude-modified D13 correctly accounts for the magnitude-scaling of the observed data.
395 Note that distance-dependent trends in the intra-event residuals of the distance- and magnitude-modified
396 D13 are also found to be negligible.

397 Coefficients of the distance- and magnitude-modified D13 (henceforth referred to as CWB19) are provided
398 in Table 3, for all ground motion intensity measures examined. Figure 11 provides regional median *PGV*
399 predictions of the GMPE related to two hypothetical scenario earthquakes at the PNR shale gas site, which
400 are equivalent in size to the two largest events that occurred during operations there in 2019. The applicability
401 of CWB19 is limited to hypocentral distances between approximately 2 and 6 km, and (positive) moment
402 magnitudes less than 3, given the sparsity of available calibration data for other values. CWB19 nevertheless
403 represents a reasonable first attempt at modelling ground motions related to UK shale gas exploration, and
404 will be refined in the future as further data are recorded.

405 **4.1 Comparing CWB19 with existing GMPEs**

406 We now examine the distance-scaling, the magnitude-scaling, and the standard deviations of CWB19, relative
407 to those of the GMPEs previously assessed for suitability to modelling the ground motions of interest. A15

408 is site corrected to a V_{s30} value of 280 m/s in all distance- and magnitude-scaling comparisons. It should
409 also be noted, as part of interpreting the comparisons, that ground motion amplitudes calculated according
410 to A15 are not strictly equivalent to those calculated using the other GMPEs (see **Data Used** for more
411 details).

412 Figure 12 compares the distance-scaling of the median predicted amplitudes of CWB19 with those of
413 the previously examined GMPEs, for a fixed focal depth of 2 km and a moment magnitude of 1.5. The
414 ground motion amplitudes predicted by the GMPEs derived from naturally occurring events (i.e. the ASB14
415 equations) are significantly larger than those predicted by the GMPEs designed for induced earthquakes (i.e.
416 all other equations examined) across most distances and intensity measures of interest. This is not surprising,
417 given that the ASB14 equations have undergone the largest extrapolation from their range of applicability
418 (e.g. Baltay and Hanks, 2014). The very near-source predicted amplitudes of CWB19 are significantly larger
419 than those of A15 and D13 (and even those of both ASB14 equations for *PGV*). The distance attenuation
420 of CWB19 is faster than that of all other examined GMPEs, such that its predictions are similar to those of
421 either A15 or D13 at the farthest distances considered. We can conclude that, for the ground motion intensity
422 measures studied, close-distance intensities predicted by CWB19 are larger than those expected by the two
423 GMPEs focused on induced events (as well as those expected by the GMPEs derived from naturally-occurring
424 events for *PGV*), but its predicted intensities at farther distances are in line with expectations for induced
425 earthquakes. This may be explained by the fact that the UK induced earthquakes examined occurred at
426 shallower depths than those used to constrain D13 and A15; all PNR and NO earthquakes occurred at depths
427 less than 3 km, while the mean focal depth of earthquakes used to fit D13 is approximately 5 km, based on
428 visual inspection of Figure 1 in Douglas et al. (2013), and the mean focal depth of earthquakes used to fit
429 A15 is 9 km (Atkinson, 2015).

430 Figure 13 compares the magnitude-scaling of the median predicted amplitudes of CWB19 with those of
431 the previously assessed GMPEs, at a distance of 3 km (which is hypocentral or epicentral, depending on
432 the functional form of the GMPE). Across all intensity measures examined except *PGV*, the ground motion
433 amplitudes predicted by the natural GMPEs are notably larger than those predicted by the induced GMPEs
434 for magnitudes less than approximately 2.5, but are similar at greater magnitudes. The magnitude-scaling

435 of CWB19 is comparable to that of D13 for PGA , $SA_{0.05}$, and $SA_{0.1}$, and that of A15 for $SA_{0.2}$; the only
 436 notable difference is a marginally steeper scaling for CWB19 in the case of $SA_{0.05}$, $SA_{0.1}$, and $SA_{0.2}$, such
 437 that expected ground motion amplitudes are higher for CWB19 than for either D13 or A15 at the largest
 438 magnitudes considered. The magnitude-scaling of CWB19 for PGV is significantly different to that of the
 439 other GMPEs at very small magnitudes, but very similar to those of ASB14_{epi}, A15, and D13 for magnitudes
 440 greater than 1.5. We conclude that the magnitude scaling of CWB19 is generally in line with that of other
 441 induced GMPEs, for the ground motion intensity measures examined.

442 Figure 14 shows intra- and inter-event standard deviation values (in natural log units) for CWB19 across
 443 all ground motion intensity measures of interest, compared with equivalent values for the other GMPEs
 444 examined. Inter-event values for CWB19 are consistently lower than those of A15 and D13, and are signifi-
 445 cantly less than those for all other GMPEs assessed in the case of PGV and $SA_{0.1}$. These findings are not
 446 surprising, given that CWB19 is derived using (essentially) only two sources, i.e. the shale gas site at PNR
 447 and the coal mine at NO. The intra-event variability values of the developed GMPE are generally slightly
 448 lower than those of the other GMPEs; this may be explained by the narrow near-source distance range of
 449 interest for CWB19. Note that the relatively small standard deviation values underline the fact that CWB19
 450 should not be used outside the seismicity context for which it was created nor the magnitude and distance
 451 ranges outlined in **Developing a Modified GMPE**, as underestimating variability in ground motions can
 452 have a significant impact on the results of seismic hazard analyses (Bommer and Abrahamson, 2006).

453 4.1.1 Improvement in GMPE

454 We can use the EMD_{total} metric developed to quantify the improvement in modelling accuracy offered by
 455 CWB19 over D13 for the data of interest, given that the scale of the score is consistent across all GMPEs.
 456 The percentage improvement is calculated as follows:

$$\% \text{ Improvement} = \frac{(EMD_{total})_{D13} - (EMD_{total})_{CWB19}}{(EMD_{total})_{D13}} \times 100 \quad (15)$$

457 where $(EMD_{total})_z$ is EMD_{total} for the GMPE z . Table 4 contains percentage improvement values for all
 458 ground motion intensity measures examined in this study. It can be seen that there is a notable improvement

459 for all intensity measures, with an average improvement of 66%. Thus, adjusting the coefficients of D13 has
460 significantly enhanced its suitability to modelling ground motions induced by UK shale gas exploration.

461 5 Conclusions

462 This paper has proposed a new method for evaluating the suitability of GMPEs to modelling the ground
463 motions in a given region of interest. The method leverages a statistical tool from sensitivity analysis to
464 quantitatively compare the distribution of residuals from a GMPE with the distribution expected for an
465 exact fit of the equation to the underlying observations. The proposed method has a number of advantages
466 over similar procedures in the literature. For example, it is based on an intuitive scoring system that yields
467 consistent score values across all GMPEs and observed datasets. It does not rely on statistical hypothesis
468 testing, from which it is difficult to measure the importance of a result. It also correctly accounts for the
469 hierarchical structure of GMPEs. The accuracy of the proposed procedure can be hampered by very small
470 sample sizes (i.e. on the order of 4 earthquakes), however such limited datasets are far from those expected
471 to be used in real-life evaluations of GMPEs.

472 The proposed evaluation procedure was used to assess the suitability of a number of different GMPEs
473 ($ASB14_{\text{hypo}}$, ASB_{epi} , A15, and D13) for modelling earthquakes induced by shale gas exploration in the
474 UK. We specifically focused on events related to the PNR shale gas site near Blackpool in Lancashire,
475 and supplemented the dataset with information on a sequence of similar events related to coal-mining that
476 occurred within the same geologic formation at New Ollerton, North Nottinghamshire. We found that D13
477 was the most applicable GMPE of the four, at least for the considered ground motion intensity measures
478 of PGV , PGA , $SA_{0.05}$, $SA_{0.1}$, and $SA_{0.2}$, and the dataset of observed recordings examined. We further
479 enhanced the suitability of D13 for modelling ground motions associated with UK shale gas exploration, by
480 adjusting its coefficients in line with the observed dataset; details of the modified equation (CWB19) are
481 provided in **Developing a Modified GMPE**.

482 This paper provides a useful tool for ranking GMPEs that can be used to select suitable candidate models
483 for input to probabilistic seismic hazard analyses (PSHA). Our assessment and development of GMPEs for
484 modelling ground motions related to UK shale gas exploration enhances understanding of the strength of

485 ground shaking associated with this type of seismicity, and the findings have many potential applications
486 in further related work. For example, the developed GMPE could be used as part of future PSHA studies
487 related to UK shale gas seismicity, for accurately modelling ground motion amplitudes at close distances and
488 small magnitudes. These studies could ultimately inform engineering seismic risk calculations, which could
489 be used to aid decision-making related to UK regulations on shale gas operations.

490 **6 Data and Resources**

491 Earthquake catalogs were obtained from the earthquake database of the British Geological Survey ([https://](https://earthquakes.bgs.ac.uk/earthquakes/dataSearch.html)
492 earthquakes.bgs.ac.uk/earthquakes/dataSearch.html). Seismograms, phase measurements, and data
493 used to correct for instrument response were acquired from the British Geological Survey’s seismic database
494 and the UK Oil and Gas Authority’s database on 2018 PNR operations ([https://www.ogauthority.co.uk/](https://www.ogauthority.co.uk/onshore/onshore-reports-and-data/preston-new-road-pnr-1z-hydraulic-fracturing-operations-data/)
495 [onshore/onshore-reports-and-data/preston-new-road-pnr-1z-hydraulic-fracturing-operations-data/](https://www.ogauthority.co.uk/onshore/onshore-reports-and-data/preston-new-road-pnr-1z-hydraulic-fracturing-operations-data/)).
496 All other data used were retrieved from sources listed in the references.

497 **7 Acknowledgements**

498 We thank Dr. Julian J. Bommer and an anonymous reviewer for very helpful comments that significantly
499 improved the quality of this manuscript. This work has been funded by the Natural Environment Research
500 Council (NERC) Grant Number NE/R017956/1 “Evaluation, Quantification and Identification of Pathways
501 and Targets for the assessment of Shale Gas RISK (EQUIPT4RISK)”, the Bristol University Microseismic
502 Projects (BUMPS), and the British Geological Survey.

503 **References**

504 Abrahamson, N. A. and R. Youngs (1992). A stable algorithm for regression analyses using the random
505 effects model, Bull. Seismol. Soc. Am. **82**(1), 505–510.

506 Akkar, S. and J. J. Bommer (2007). Empirical prediction equations for peak ground velocity derived from
507 strong-motion records from Europe and the Middle East, Bull. Seismol. Soc. Am. **97**(2), 511–530.

508 Akkar, S., M. Sandikkaya, and J. Bommer (2014a). Empirical ground-motion models for point-and extended-
509 source crustal earthquake scenarios in Europe and the Middle East, Bull. Earthquake Eng. **12**(1), 359–387.

510 Akkar, S., M. Sandikkaya, M. Şenyurt, A. A. Sisi, B. Ay, P. Traversa, J. Douglas, F. Cotton, L. Luzi,
511 B. Hernandez, et al. (2014b). Reference database for seismic ground-motion in Europe (RESORCE), Bull.
512 Earthquake Eng. **12**(1), 311–339.

513 Ambraseys, N., J. Douglas, S. Sarma, and P. Smit (2005). Equations for the estimation of strong ground
514 motions from shallow crustal earthquakes using data from Europe and the Middle East: horizontal peak
515 ground acceleration and spectral acceleration, Bull. Earthquake Eng. **3**(1), 1–53.

516 Ancheta, T. D., R. B. Darragh, J. P. Stewart, E. Seyhan, W. J. Silva, B. S. Chiou, K. E. Wooddell, R. W.
517 Graves, A. R. Kottke, D. M. Boore, et al. (2014). NGA-West2 database, Earthquake Spectra **30**(3),
518 989–1005.

519 Arup (2014). Temporary shale gas exploration, Preston New Road, Lancashire: Environmental Statement.

520 Atkinson, G. M. (2008). Ground-motion prediction equations for eastern North America from a referenced
521 empirical approach: Implications for epistemic uncertainty, Bull. Seismol. Soc. Am. **98**(3), 1304–1318.

522 Atkinson, G. M. (2015). Ground-motion prediction equation for small-to-moderate events at short hypocen-
523 tral distances, with application to induced-seismicity hazards, Bull. Seismol. Soc. Am. **105**(2A), 981–992.

524 Atkinson, G. M. and M. Morrison (2009). Observations on regional variability in ground-motion amplitudes
525 for small-to-moderate earthquakes in North America, Bull. Seismol. Soc. Am. **99**(4), 2393–2409.

526 Baltay, A. S. and T. C. Hanks (2014). Understanding the magnitude dependence of PGA and PGV in
527 NGA-West 2 data, Bull. Seismol. Soc. Am. **104**(6), 2851–2865.

528 Beauval, C., H. Tasan, A. Laurendeau, E. Delavaud, F. Cotton, P. Guéguen, and N. Kuehn (2012). On
529 the testing of ground-motion prediction equations against small-magnitude data, Bull. Seismol. Soc.
530 Am. **102**(5), 1994–2007.

531 Bommer, J. J. and N. A. Abrahamson (2006). Why do modern probabilistic seismic-hazard analyses often
532 lead to increased hazard estimates?, Bull. Seismol. Soc. Am. **96**(6), 1967–1977.

533 Bommer, J. J., J. Douglas, F. Scherbaum, F. Cotton, H. Bungum, and D. Fah (2010). On the selection of
534 ground-motion prediction equations for seismic hazard analysis, Seismol. Res. Lett. **81**(5), 783–793.

535 Bommer, J. J., P. J. Stafford, J. E. Alarcón, and S. Akkar (2007). The influence of magnitude range on
536 empirical ground-motion prediction, Bull. Seismol. Soc. Am. **97**(6), 2152–2170.

537 Boore, D. M. (2010). Orientation-independent, nongeometric-mean measures of seismic intensity from two
538 horizontal components of motion, Bull. Seismol. Soc. Am. **100**(4), 1830–1835.

539 Bourne, S., S. Oates, J. Bommer, B. Dost, J. Van Elk, and D. Doornhof (2015). A Monte Carlo method for
540 probabilistic hazard assessment of induced seismicity due to conventional natural gas production, Bull.
541 Seismol. Soc. Am. **105**(3), 1721–1738.

542 Bradley, B. A. (2013). A New Zealand-specific pseudospectral acceleration ground-motion prediction equation
543 for active shallow crustal earthquakes based on foreign models, Bull. Seismol. Soc. Am. **103**(3), 1801–1822.

544 Butcher, A., R. Lockett, J.-M. Kendall, and B. Baptie (2019). Corner frequencies, seismic moments and
545 earthquake magnitudes: The effects of high-frequency attenuation on microseismicity, Bull. Seismol. Soc.
546 Am. (submitted).

547 Butcher, A., R. Lockett, J. P. Verdon, J.-M. Kendall, B. Baptie, and J. Wookey (2017). Local magnitude
548 discrepancies for near-event receivers: Implications for the UK traffic-light scheme, Bull. Seismol. Soc.
549 Am. **107**(2), 532–541.

550 Campbell, N., C. Fenton, and S. Tallett-Williams (2016). An Investigation into the Effects of Material
551 Properties on Shear Wave Velocity in Rocks/Soils. In Proceedings of the 5th International Conference on
552 Geotechnical and Geophysical Site Characterization ISC-5, Gold Coast, Australia.

553 Chiou, B., R. Youngs, N. Abrahamson, and K. Addo (2010). Ground-motion attenuation model for small-to-
554 moderate shallow crustal earthquakes in California and its implications on regionalization of ground-motion
555 prediction models, Earthquake spectra **26**(4), 907–926.

556 Chiou, B. S.-J. and R. R. Youngs (2014). Update of the Chiou and Youngs NGA model for the average
557 horizontal component of peak ground motion and response spectra, Earthquake Spectra **30**(3), 1117–1153.

558 Chun, M.-H., S.-J. Han, and N.-I. Tak (2000). An uncertainty importance measure using a distance metric
559 for the change in a cumulative distribution function, Reliab. Eng. Syst. Saf. **70**(3), 313–321.

560 Clarke, H., L. Eisner, P. Styles, and P. Turner (2014). Felt seismicity associated with shale gas hydraulic
561 fracturing: The first documented example in Europe, Geophys. Res. Lett. **41**(23), 8308–8314.

562 Clarke, H., J. P. Verdon, T. Kettlety, A. Baird, and J.-M. Kendall (2019). Real-time imaging, forecasting,
563 and management of human-induced seismicity at Preston New Road, Lancashire, England, Seismol. Res.
564 Lett. **90**(5), 1902–1915.

565 Cremen, G., M. J. Werner, and B. Baptie (2019). Understanding induced seismicity hazard related to shale
566 gas exploration in the UK. In SECED 2019 Conference: Earthquake Risk and Engineering towards a
567 Resilient World.

568 Douglas, J., B. Edwards, V. Convertito, N. Sharma, A. Tramelli, D. Kraaijpoel, B. M. Cabrera, N. Maercklin,
569 and C. Troise (2013). Predicting ground motion from induced earthquakes in geothermal areas, Bull.
570 Seismol. Soc. Am. **103**(3), 1875–1897.

571 Douglas, J. and P. Jousset (2011). Modeling the difference in ground-motion magnitude-scaling in small and
572 large earthquakes, Seismol. Res. Lett. **82**(4), 504–508.

573 Haney, M. M., J. Power, M. West, and P. Michaels (2012). Causal instrument corrections for short-period
574 and broadband seismometers, Seismol. Res. Lett. **83**(5), 834–845.

575 Jiang, J. (2007). Linear and generalized linear mixed models and their applications. Springer Science &
576 Business Media.

577 Kale, Ö. and S. Akkar (2013). A new procedure for selecting and ranking ground-motion prediction equations
578 (GMPEs): The Euclidean distance-based ranking (EDR) method, Bull. Seismol. Soc. Am. **103**(2A), 1069–
579 1084.

580 Kwak, S. G. and J. H. Kim (2017). Central limit theorem: the cornerstone of modern statistics, Korean J.
581 Anesthesiol. **70**(2), 144.

582 Laird, N. (2004). Chapter 5: Random effects and the linear mixed model, Volume 8 of Regional Conference
583 Series in Probability and Statistics, pp. 79–95. Beechwood OH and Alexandria VA: Institute of Mathe-
584 matical Statistics and American Statistical Association.

585 Lee, S.-Y. and X.-Y. Song (2004). Evaluation of the Bayesian and maximum likelihood approaches in
586 analyzing structural equation models with small sample sizes, Multivariate Behav. Res. **39**(4), 653–686.

587 Lindley, D. V. (1991). Making Decisions (2 ed.). John Wiley & Sons.

588 Mak, S., R. A. Clements, and D. Schorlemmer (2014). Comment on “A new procedure for selecting and
589 ranking ground-motion prediction equations (GMPEs): The Euclidean distance-based ranking (EDR)
590 method” by Özkan Kale and Sinan Akkar, Bull. Seismol. Soc. Am. **104**(6), 3139–3140.

591 Mak, S., R. A. Clements, and D. Schorlemmer (2017). Empirical evaluation of hierarchical ground-motion
592 models: Score uncertainty and model weighting, Bull. Seismol. Soc. Am. **107**(2), 949–965.

593 Ornthammarath, T., J. Douglas, R. Sigbjörnsson, and C. G. Lai (2011). Assessment of ground motion
594 variability and its effects on seismic hazard analysis: A case study for Iceland, Bull. Earthquake Eng. **9**(4),
595 931–953.

596 Perron, V., A. Laurendeau, F. Hollender, P.-Y. Bard, C. Gélis, P. Traversa, and S. Drouet (2018). Selecting
597 time windows of seismic phases and noise for engineering seismology applications: A versatile methodology
598 and algorithm, Bull. Earthquake Eng. **16**(6), 2211–2225.

599 Scasserra, G., J. P. Stewart, P. Bazzurro, G. Lanzo, and F. Mollaioli (2009). A comparison of NGA ground-
600 motion prediction equations to Italian data, Bull. Seismol. Soc. Am. **99**(5), 2961–2978.

601 Scherbaum, F., F. Cotton, and P. Smit (2004). On the use of response spectral-reference data for the selection
602 and ranking of ground-motion models for seismic-hazard analysis in regions of moderate seismicity: The
603 case of rock motion, Bull. Seismol. Soc. Am. **94**(6), 2164–2185.

604 Scherbaum, F., E. Delavaud, and C. Riggelsen (2009). Model selection in seismic hazard analysis: An
605 information-theoretic perspective, Bull. Seismol. Soc. Am. **99**(6), 3234–3247.

606 Selley, R. C. (2012). UK shale gas: the story so far, Mar Petrol Geol **31**(1), 100–109.

607 Seyhan, E. and J. P. Stewart (2014). Semi-empirical nonlinear site amplification from NGA-West2 data and
608 simulations, Earthquake Spectra **30**(3), 1241–1256.

609 Stafford, P. J. (2015). Extension of the random-effects regression algorithm to account for the effects of
610 nonlinear site response, Bull. Seismol. Soc. Am. **105**(6), 3196–3202.

611 Stafford, P. J., F. O. Strasser, and J. J. Bommer (2008). An evaluation of the applicability of the NGA models
612 to ground-motion prediction in the Euro-Mediterranean region, Bull. Earthquake Eng. **6**(2), 149–177.

613 Stewart, J. P., J. Douglas, M. Javanbarg, Y. Bozorgnia, N. A. Abrahamson, D. M. Boore, K. W. Campbell,
614 E. Delavaud, M. Erdik, and P. J. Stafford (2015). Selection of ground motion prediction equations for the
615 global earthquake model, Earthquake Spectra **31**(1), 19–45.

616 Verdon, J. P., J.-M. Kendall, A. Butcher, R. Lockett, and B. J. Baptie (2017). Seismicity induced by longwall
617 coal mining at the Thoresby Colliery, Nottinghamshire, UK, Geophys. J. Int. **212**(2), 942–954.

618 Villani, C. (2008). Optimal transport: old and new, Volume 338. Springer Science & Business Media.

619 Wang, L.-J. (1996). Processing of near-field earthquake accelerograms, California Institute of Technology.

620 Wasserstein, R. L. and N. A. Lazar (2016). The ASA’s statement on p-values: context, process, and purpose,
621 The American Statistician **70**(2), 129–133.

Tables

Table 1: Scores calculated using the proposed procedure, for the cases in Examples 1-3 of Mak et al. (2017).

Example	Case	EMD_{total}	$\ell\ell(\mathbf{p}, \mathbf{V}, \mathbf{q})$
1	Case 1	0.25	38.8
	Case 2	0.39	38.5
2	Correct	0.25	61.2
	Biased	0.48	61.5
3	Correct	0.25	38.8
	Inflated σ_b	0.35	39.6
	Deflated σ_b	0.17	39.1

$\ell\ell(\mathbf{p}, \mathbf{V}, \mathbf{q})$ scores of the Mak et al. (2017) procedure are also shown for comparison. Note that the smallest score for a given procedure (marked in bold) indicates the best model.

Table 2: Ranking of GMPEs for suitability to modelling ground motions produced by UK shale gas-related seismicity, using both the proposed procedure and the procedure of Mak et al. (2017).

Intensity Measure	Metric	ASB14 _{hypo}	ASB14 _{epi}	A15	D13
<i>PGA</i>	EMD_{total}	4.56	3.47	1.48	0.74
	$\ell\ell(\mathbf{p}, \mathbf{V}, \mathbf{q})$	1830	1297	569	505
<i>PGV</i>	EMD_{total}	1.88	0.95	1.25	0.92
	$\ell\ell(\mathbf{p}, \mathbf{V}, \mathbf{q})$	763	605	493	645
<i>SA</i> _{0.05}	EMD_{total}	4.64	3.63	1.39	0.62
	$\ell\ell(\mathbf{p}, \mathbf{V}, \mathbf{q})$	1912	1428	610	550
<i>SA</i> _{0.1}	EMD_{total}	4.82	3.78	1.54	1.17
	$\ell\ell(\mathbf{p}, \mathbf{V}, \mathbf{q})$	1912	1404	571	535
<i>SA</i> _{0.2}	EMD_{total}	5.31	4.26	1.06	1.81
	$\ell\ell(\mathbf{p}, \mathbf{V}, \mathbf{q})$	2178	1579	474	605

Note that the smallest score for a given procedure (marked in bold) indicates the best model.

Table 3: Coefficients of CWB19 for all ground motion intensity measures (IMs) examined. Note that the functional form of the GMPE is presented in equation 11.

IM	a	b	c	h	d	ϕ	τ	σ
<i>PGA</i>	-5.096	2.146	-2.611	constrained to zero	-0.023	0.563	0.437	0.712
<i>PGV</i>	-10.213	2.913	-2.719	constrained to zero	-0.046	0.553	0.158	0.575
<i>SA</i> _{0.05}	-5.027	2.717	-2.890	constrained to zero	-0.008	0.696	0.378	0.792
<i>SA</i> _{0.1}	-4.988	2.814	-2.723	constrained to zero	-0.039	0.632	0.227	0.672
<i>SA</i> _{0.2}	-7.704	3.639	-2.276	constrained to zero	-0.057	0.549	0.430	0.698

Table 4: Percentage improvement in modelling accuracy offered by CWB19 over D13 for the data of interest in this study.

IM	$(EMD_{total})_{CWB19}$	$(EMD_{total})_{D13}$	% Improvement
<i>PGA</i>	0.21	0.74	72
<i>PGV</i>	0.48	0.92	48
<i>SA_{0.05}</i>	0.26	0.62	58
<i>SA_{0.1}</i>	0.40	1.17	66
<i>SA_{0.2}</i>	0.25	1.81	86

Note that IM stands for ground motion intensity measure. Values for $(EMD_{total})_{D13}$ are taken from Table 2.

623 Figures

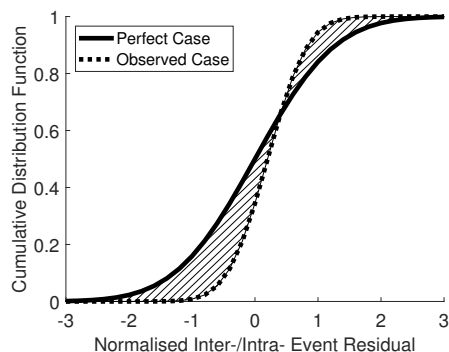


Figure 1: A graphical representation of the scoring system for our proposed GMPE evaluation procedure, which quantifies the distance between the CDF of the standard normal distribution (perfect case) and that of the maximum likelihood normal distribution (observed case) for each type of normalised residual. $\mu_x = 0.5$ and $\sigma_x = 0.5$ for the observed case, therefore $EMD_x = \sqrt{0.5^2 + (0.5 - 1)^2} = 0.7$ in this case.

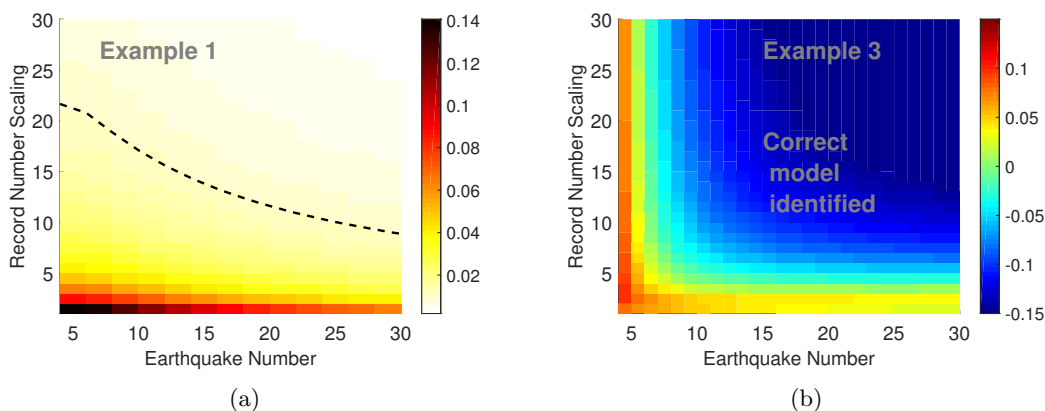


Figure 2: Understanding the sample sizes necessary for the proposed evaluation procedure to perform correctly in Examples 1 and 3 of Mak et al. (2017). (a) Absolute difference between the EMD_{total} values for Case 1 and Case 2 in Example 1, (black dashed line indicates a value of 0.01) and (b) difference between the EMD_{total} values for the correct model and the model with deflated σ_b , as a function of earthquake number and the scaling of record number per earthquake. Note that lighter colours in (a) and darker blue colours in (b) indicate a more correct performance of the score.

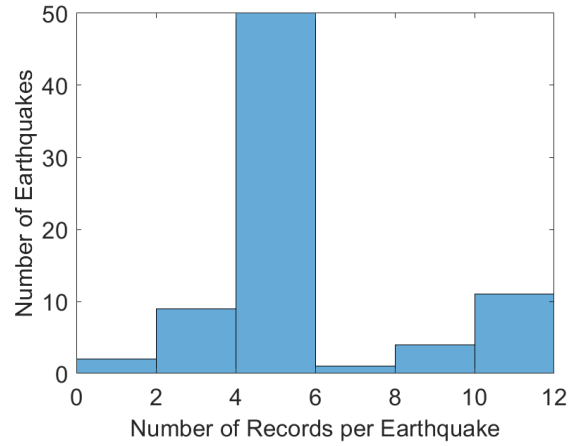


Figure 3: Histogram of the complete observed ground motion record database used in this study.

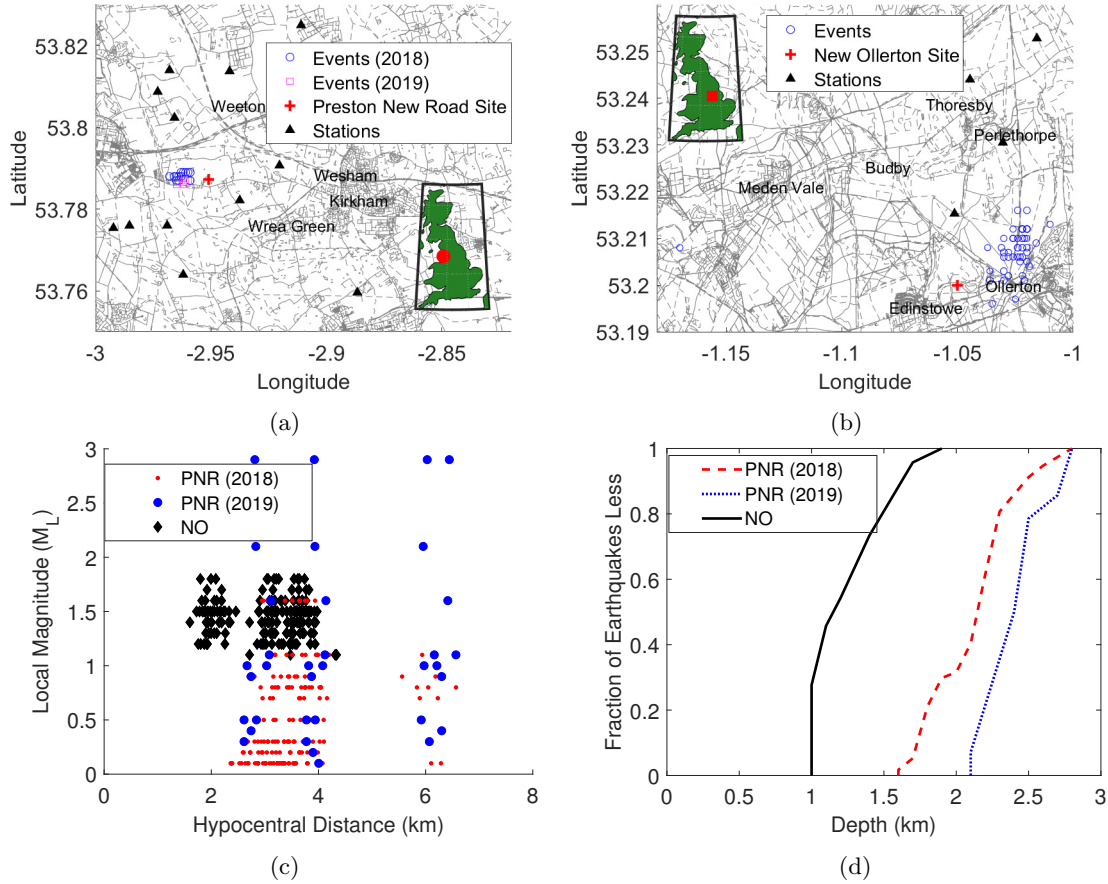


Figure 4: A summary of the data examined in this study. (a) Locations of the considered seismicity and seismic monitoring stations for the Preston New Road (PNR) shale gas site in Lancashire and (b) the Thoresby Colliery at New Ollerton (NO), North Nottinghamshire (insets highlight locations relative to all of Great Britain). (c) Magnitude, hypocentral distance, and (d) depth data examined.

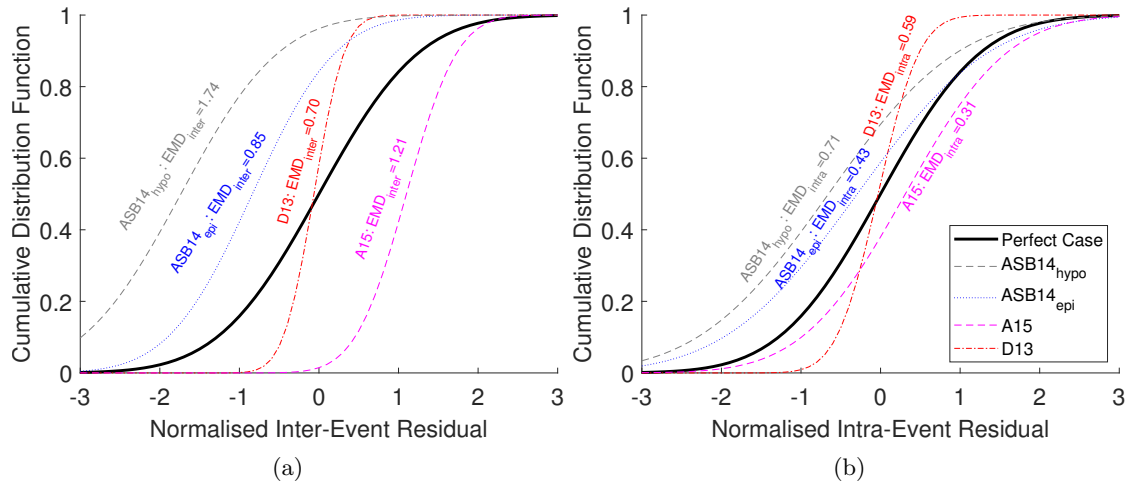


Figure 5: Normalised (a) inter- and (b) intra-event PGV residuals for the four GMPEs evaluated, compared with those expected from a standard normal distribution (the ‘Perfect Case’). Also plotted are EMD scores for each type of residual.

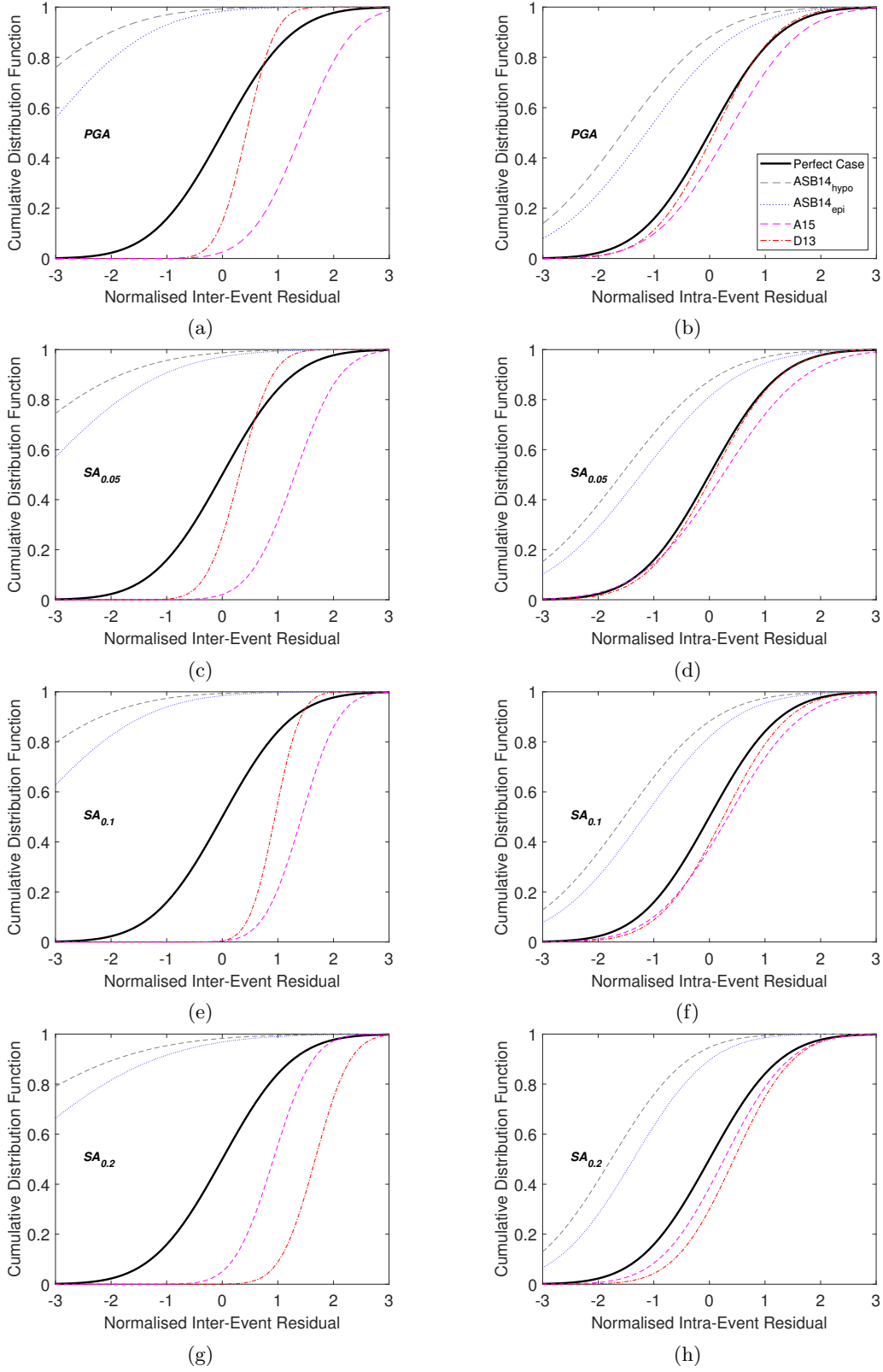


Figure 6: Normalised (a, c, e, g) inter- and (b, d, f, h) intra-event PGA , $SA_{0.05}$, $SA_{0.1}$, and $SA_{0.2}$ residuals for the four GMPEs evaluated, compared with those expected from a standard normal distribution (the 'Perfect Case').

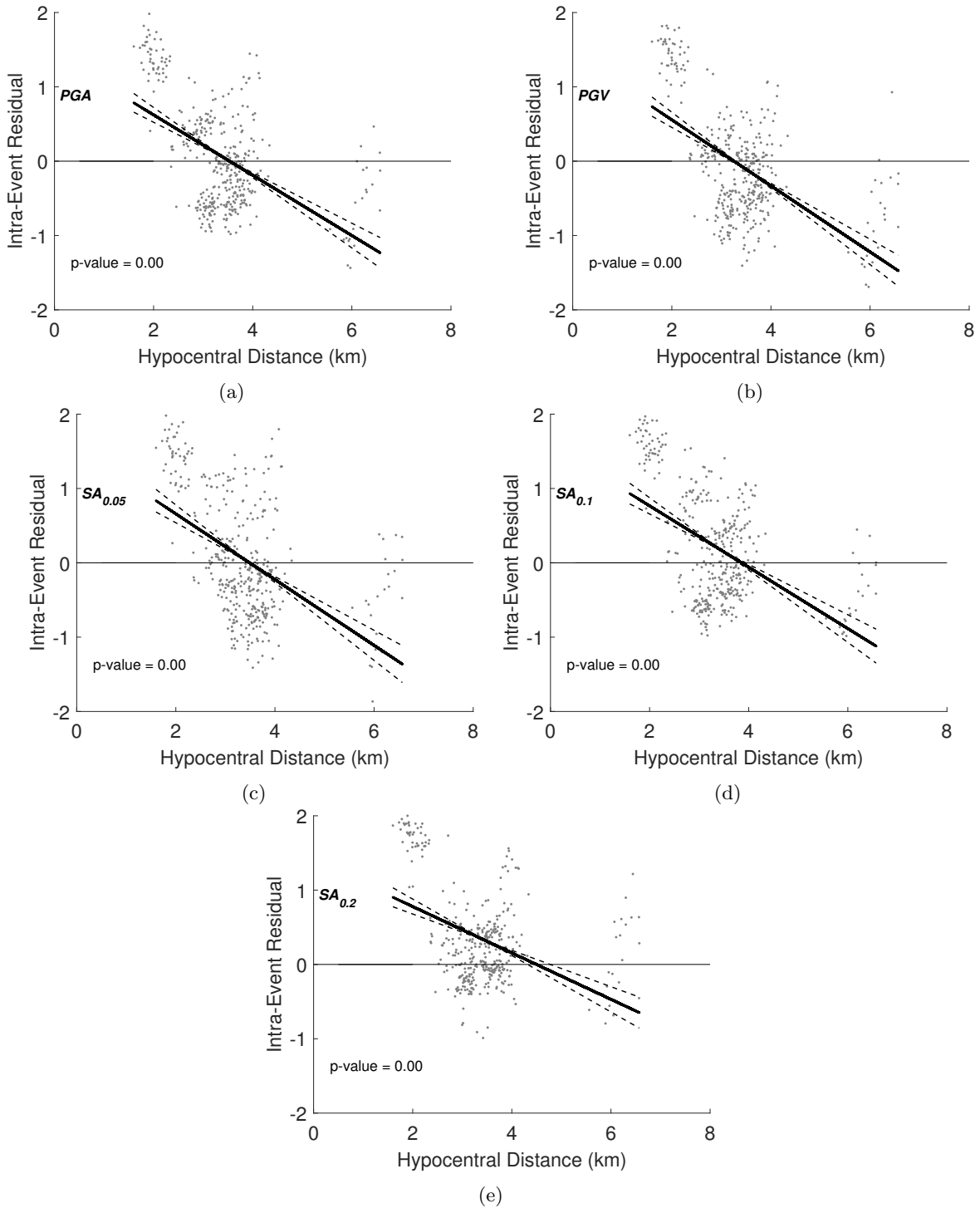


Figure 7: Variation of the D13 normalised intra-event residuals with hypocentral distance for (a) PGA , (b) PGV , (c) $SA_{0.05}$, (d) $SA_{0.1}$, and (e) $SA_{0.2}$. Also shown are the lines fit using linear regression (solid black lines) and their 95% confidence intervals (dashed lines). The p-value for a given plot tests the null hypothesis that the slope of the fitted line equals zero.

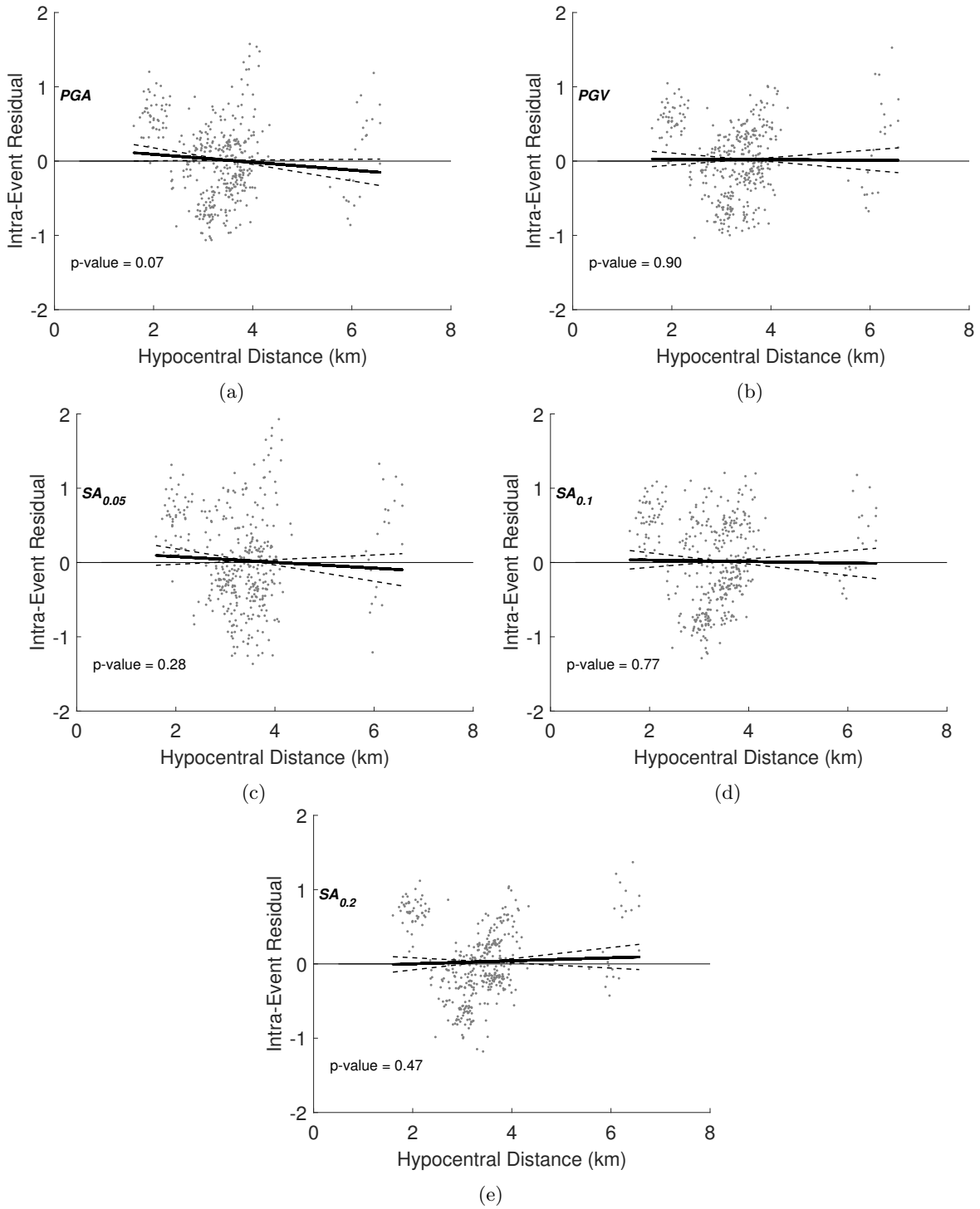


Figure 8: Variation of the distance-modified D13 normalised intra-event residuals with hypocentral distance for (a) PGA , (b) PGV , (c) $SA_{0.05}$, (d) $SA_{0.1}$, and (e) $SA_{0.2}$. Also shown are the lines fit using linear regression (solid black lines) and their 95% confidence intervals (dashed lines). The p-value for a given plot tests the null hypothesis that the slope of the fitted line equals zero.

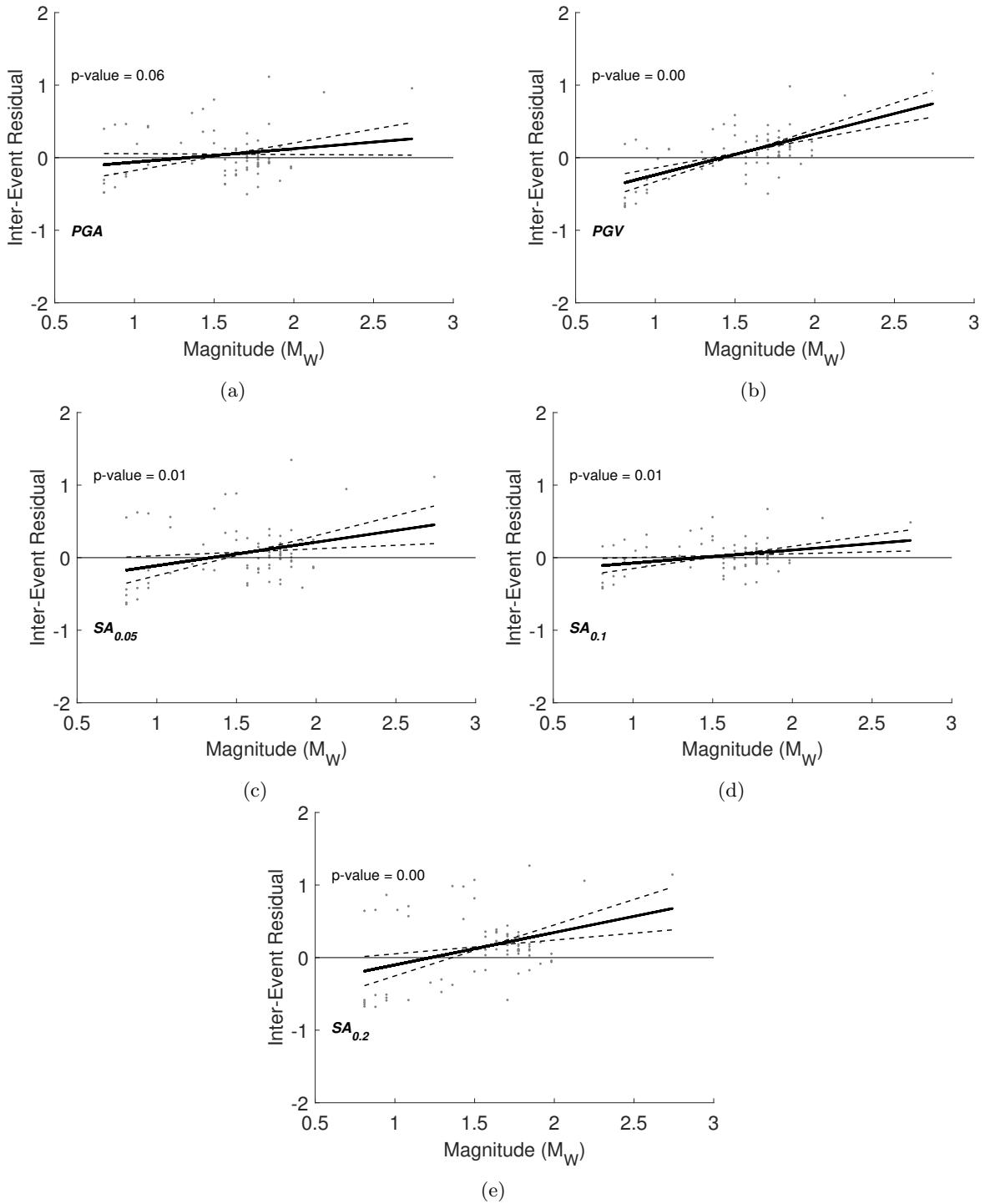


Figure 9: Variation of the distance-modified D13 normalised inter-event residuals with magnitude for (a) PGA , (b) PGV , (c) $SA_{0.05}$, (d) $SA_{0.1}$, and (e) $SA_{0.2}$. Also shown are the lines fit using linear regression (solid black lines) and their 95% confidence intervals (dashed lines). The p-value for a given plot tests the null hypothesis that the slope of the fitted line equals zero.

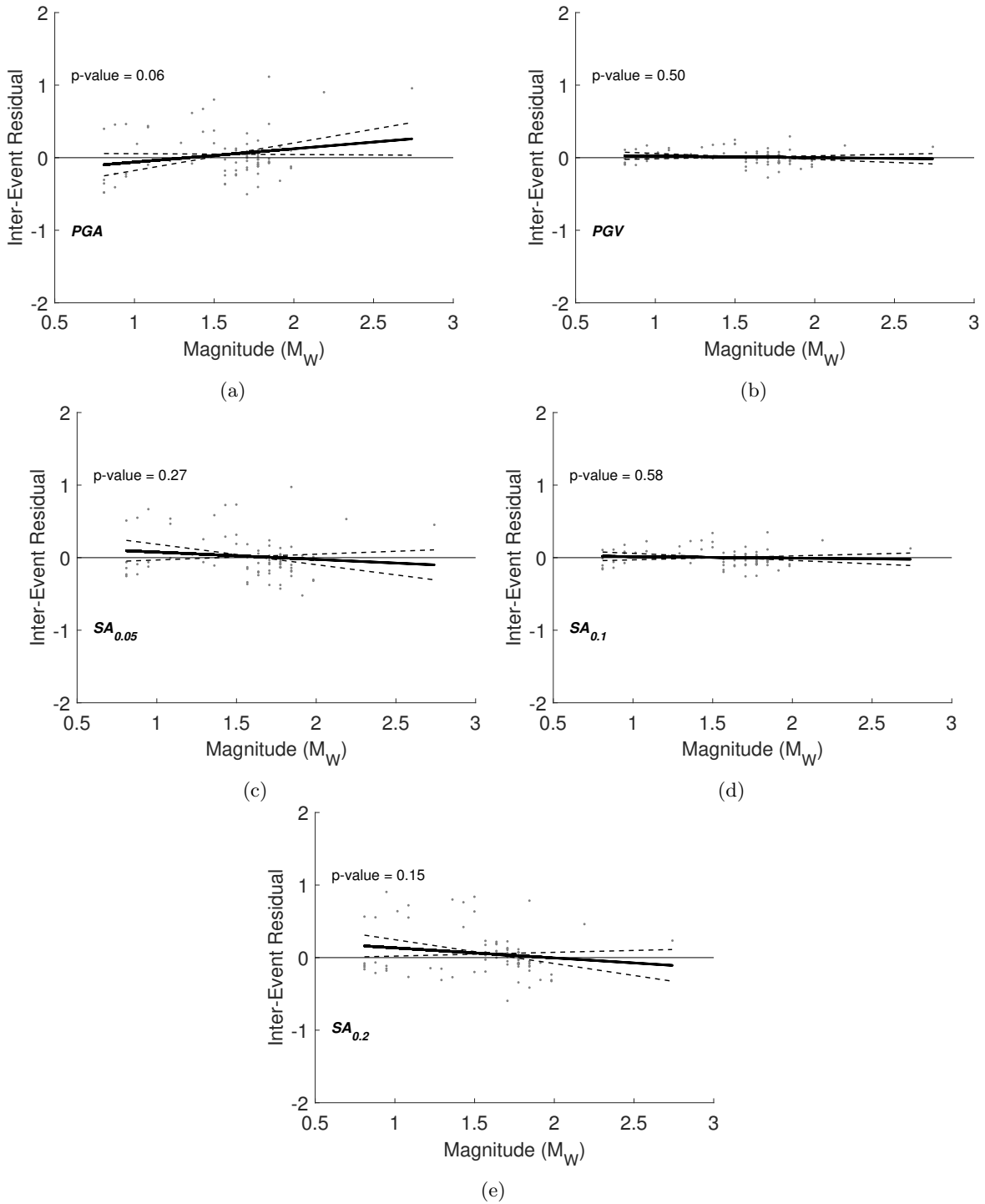
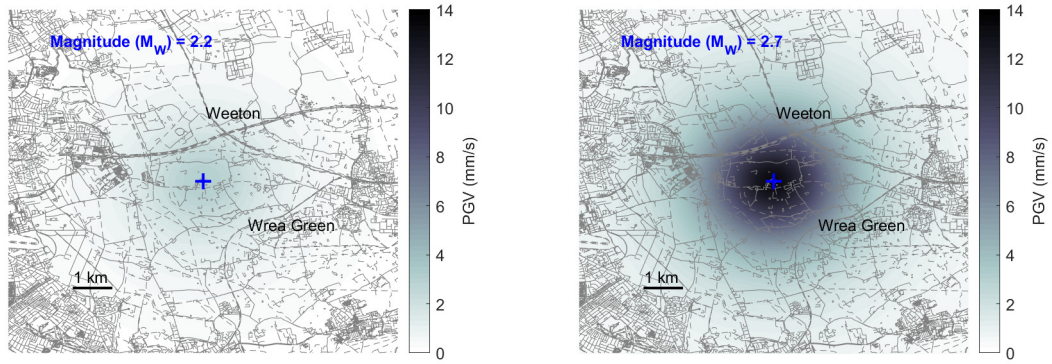


Figure 10: Variation of the CWB19 normalised inter-event residuals with magnitude for (a) PGA , (b) PGV , (c) $SA_{0.5}$, (d) $SA_{0.1}$, and (e) $SA_{0.2}$. Also shown are the lines fit using linear regression (solid black lines) and their 95% confidence intervals (dashed lines). The p-value for a given plot tests the null hypothesis that the slope of the fitted line equals zero.



(a)

(b)

Figure 11: CWB19 median predictions of PGV within the PNR greater region, for two hypothetical scenarios: (a) an earthquake with $M_w = 2.2$ and (b) an earthquake with $M_w = 2.7$, that are co-located with the PNR shale gas site (blue cross) at a depth of 2 km.

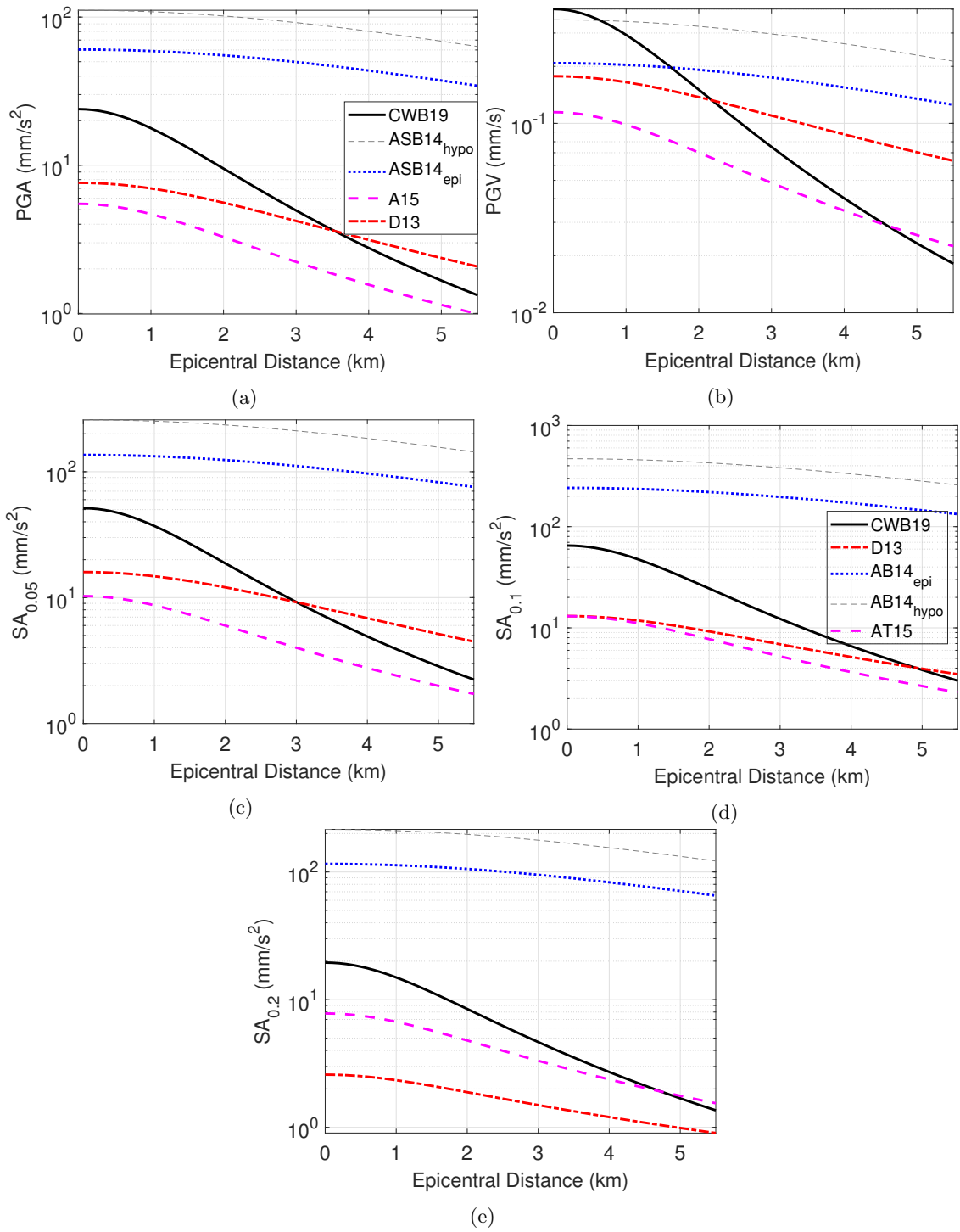


Figure 12: Distance-scaling of CWB19 for a fixed focal depth of 2 km and a moment magnitude of 1.5, compared with the equivalent distance-scaling of other GMPEs examined in this study, for (a) PGA , (b) PGV , (c) $SA_{0.05}$, (d) $SA_{0.1}$, and (e) $SA_{0.2}$.

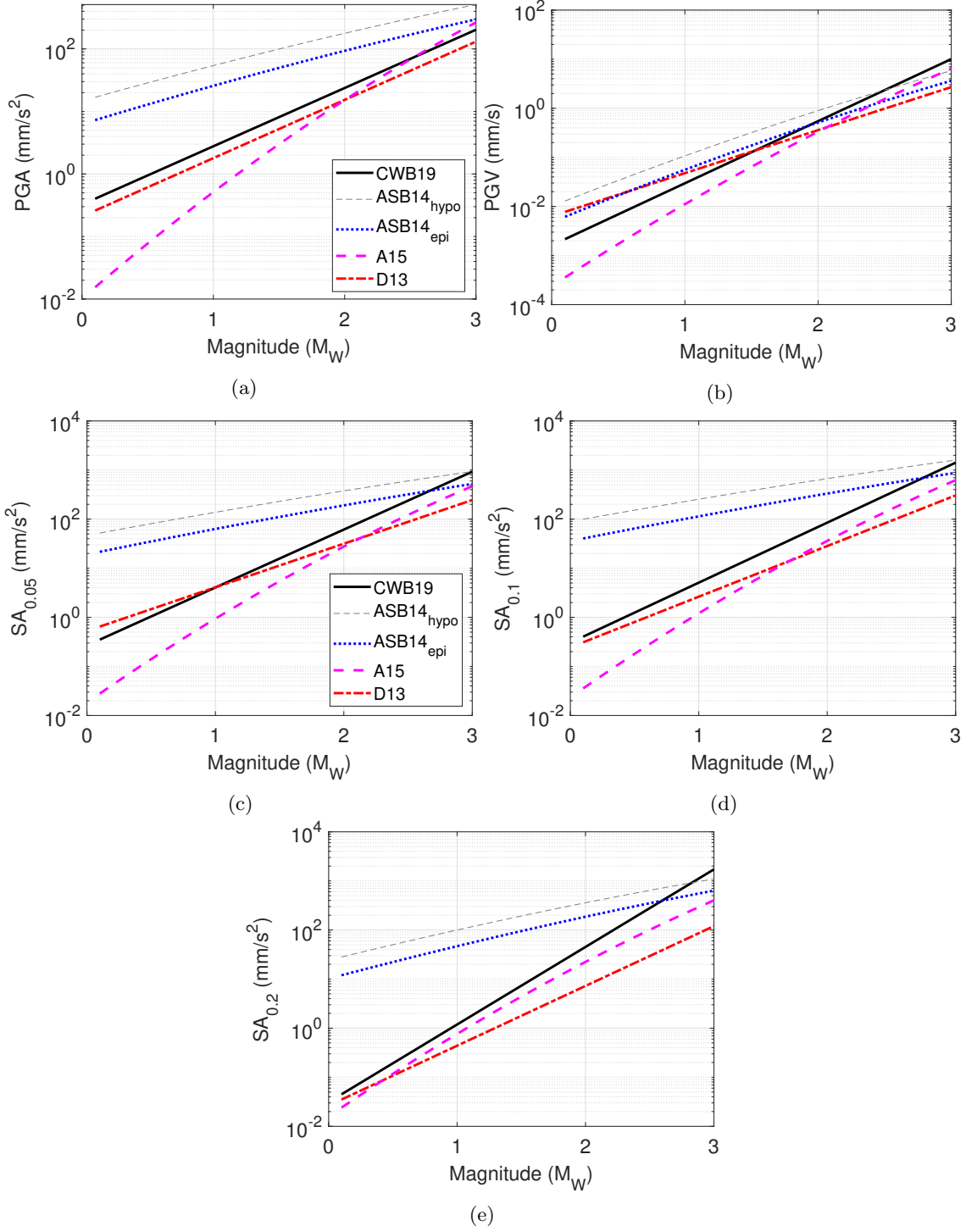


Figure 13: Magnitude-scaling of CWB19 at 3 km, compared with the equivalent magnitude-scaling of other GMPEs examined in this study, for (a) PGA , (b) PGV , (c) $SA_{0.05}$, (d) $SA_{0.1}$, and (e) $SA_{0.2}$.

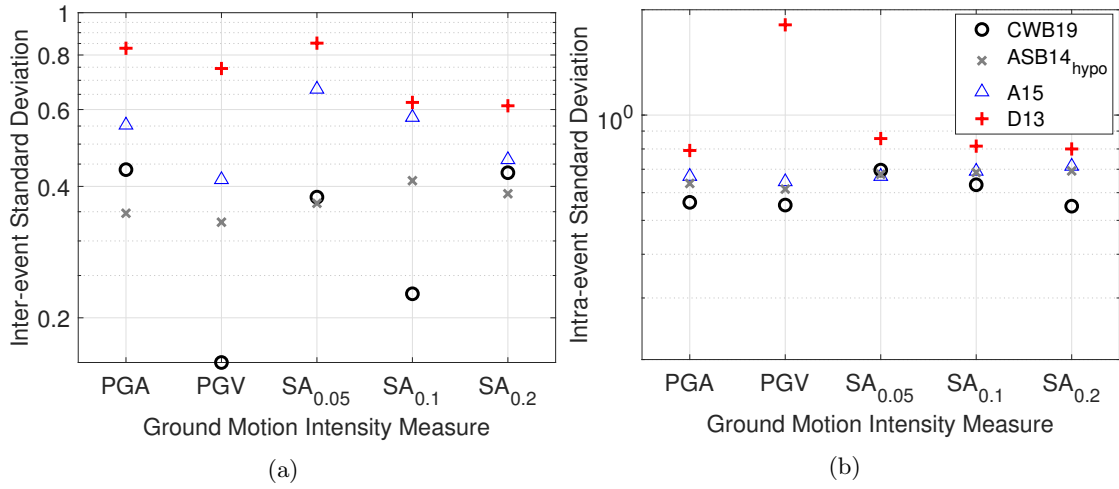


Figure 14: (a) Inter- and (b) intra-event standard deviations (in natural log units) for CWB19, compared with equivalent values for other GMPEs examined in this study. Note that ASB14_{epi} data are not included for clarity, since they are almost identical to those of ASB14_{hypo} (Akkar et al., 2014a).